

THE UNIVERSITY OF CALGARY

Strapdown INS Orientation Accuracy with GPS Aiding

by

Jan Škaloud

A THESIS

SUBMITTED TO THE FACULTY OF GRADUATE STUDIES
IN PARTIAL FULFILMENT OF THE REQUIREMENTS FOR THE
DEGREE OF MASTER OF SCIENCE

DEPARTMENT OF GEOMATICS ENGINEERING

CALGARY, ALBERTA

APRIL, 1995

© Jan Škaloud, 1995

THE UNIVERSITY OF CALGARY
FACULTY OF GRADUATE STUDIES

The undersigned certify that they have read, and recommended to the Faculty of Graduate Studies for acceptance, a thesis entitled "Strapdown INS Orientation Accuracy With GPS Aiding" submitted by Jan Škaloud in partial fulfilment of the requirements for the degree of Master of Science.

K.P. Schwarz

Supervisor, Dr. K.P. Schwarz, Department of Geomatics Engineering

M.A. Chapman

Dr. M.A. Chapman, Department of Geomatics Engineering

D.H. Manz

Dr. D.H. Manz, Department of Civil Engineering

May 1, 1995

Date

ABSTRACT

The aiding of an Inertial Navigation System (INS) with differential measurements from receivers using the Global Positioning System (GPS) is investigated for precise attitude determination in support of airborne remote sensing. The fundamental error equations of INS and GPS are presented and the effect of measurement system errors on orientation accuracy is analyzed. The update parameters of a decentralized Kalman filter for optimal attitude determination are closely examined by means of computer simulation. The orientation stability of the Litton LTN-90-100 strapdown inertial system is tested both in a well-controlled lab environment and under flight conditions. In flight, short term attitude accuracies of 15 - 30 arc seconds are achieved. In this case, the INS/GPS orientation parameters are compared to those derived from ground control via inverse photogrammetry. The feasibility of using INS/GPS derived attitude/position for a variety of airborne remote sensing applications is assessed.

ACKNOWLEDGEMENTS

I would like to express my gratitude to my supervisor, Professor Klaus-Peter Schwarz, for his continuous support, encouragement and guidance throughout my graduate studies. Dr. Michael Chapman is thanked for his valuable advice to photogrammetry related topics.

Special thanks go to my colleague Darren Cosandier for providing his professional expertise, software and help when formulating the core of this research. My friend Vladimir Argeseanu is thanked for polishing the language of this thesis, his assistance in data collection and his continued good humour. I also wish to thank to Dr. Ming Wei, Mr. Ziwen Liu, Mr. Gengsheng Zhang and Mr. Zuofa Li for many fruitful discussions and help when solving INS related problems. Garth Wanamaker expertise in performing high quality photogrammetric measurements is very much appreciated.

The financial support of this research, obtained through a Strategic Grant and an Operating Grant of the Natural Sciences and Engineering Research Council of Canada (NSERC), is gratefully acknowledged. Flying time and expertise was provided by Geodesy Remote Sensing Inc., Calgary, Alberta. This support is gratefully acknowledged.

Finally, my deepest thanks go to my parents who set the foundation on which I could build and for offering their continuous encouragement.

TABLE OF CONTENTS

APPROVAL PAGE	ii
ABSTRACT	iii
ACKNOWLEDGEMENTS	iv
TABLE OF CONTENTS	v
LIST OF TABLES	viii
LIST OF FIGURES	ix
NOTATION	xi
CHAPTER 1: INTRODUCTION	1
1.1 Background and Objective	1
1.2 Outline	5
CHAPTER 2: STRAPDOWN INERTIAL NAVIGATION SYSTEMS (SINS)	8
2.1 Principle	8
2.2 General Description	9
2.3 INS Mechanization in Earth-Centered-Earth-Fixed (ECEF) Frame	10
2.4 Orientation from a Strapdown INS	13
2.5 Initial Alignment	14
2.6 INS Measurement Error Model	16

2.6.1	Gyro Measurement Error Model	17
2.6.2	Accelerometer Measurement Error Model	17
2.7	INS Error State Model	18
CHAPTER 3: THE GLOBAL POSITIONING SYSTEM (GPS)		21
3.1	General Description	21
3.2	Observation Equations	22
3.3	Differential Observation and Residual Errors	25
3.4	GPS Error State Model	26
CHAPTER 4: THE ERROR MODEL OF INS/GPS INTEGRATION FOR PRECISE ATTITUDE DETERMINATION		28
4.1	Attitude Error Model Analysis	28
4.2	Kalman Filtering	34
4.3	Estimation of INS Attitude Errors by GPS Aiding	36
4.4	INS/GPS Integration Strategies For Precise Attitude Determination ..	40
CHAPTER 5: GPS/INS ORIENTATION ACCURACY OBTAINED VIA SIMULATION		43
5.1	Simulation Flowchart	43
5.2	Specification of Measurement System Errors	45
5.3	Attitude Errors from Simulation	47

CHAPTER 6: STABILITY OF GYROSCOPES	51
6.1 Test Design	52
6.2 Data Analysis And Results	53
CHAPTER 7: INS-GPS-PHOTOGRAMMETRY AIRBORNE TEST	56
7.1 Attitude Derived from Inverse Photogrammetry	57
7.2 INS-Camera Offset Determination	60
7.3 Equipment Selection and Test Design	63
7.4 Photogrammetric Results	65
7.5 INS/GPS Orientation Performance Analysis	67
7.6 INS/GPS Measurements Delay	71
7.7 Frequency Analysis of Inertial Data	74
CHAPTER 8: CONCLUSIONS AND RECOMMENDATIONS	80
8.1 Conclusions	80
8.2 Recommendations	82
REFERENCES	84

LIST OF TABLES

1.1	Accuracy Requirements For Airborne Application	4
5.1	Specification of Inertial Sensor Noise	45
5.2	Specification of DD GPS Position and Velocity Noise	46
5.3	INS/GPS Attitude Performance From Simulation	48
6.1	Rotation Sequence	53
7.1	Bundle Adjustment Results	66

LIST OF FIGURES

1.1	Image Georeferencing by On-Board Navigation Sensors	1
2.1	INS Body Frame	9
2.2	Inertial Mechanization Equations in Earth Fixed Frame	12
4.1	INS East Channel With GPS Velocity Aiding	37
4.2	Block Diagram of INS/GPS Integration	41
5.1	INS Attitude (Gyro Drift $0.01^\circ/\text{h}$)	50
5.2	INS Attitude with 2 Sec GPS Update (G. Drift $0.01^\circ/\text{h}$)	50
5.3	INS Attitude with 50 Sec GPS Update (G. Drift $0.01^\circ/\text{h}$)	50
6.1	LTN-90-100 on Rotation Platform	51
6.2	LTN-90-100 Relative Azimuth Determination, $\omega = 20 \text{ deg/s}$	54
6.3	Relative Azimuth Determination Without Quantizer Effect	55
6.4	Repeatability of Roll Determination at Different Azimuths	55
7.1	Equipment Being Loaded into the Airplane	56
7.2	INS-GPS-Camera Offset Determination	61
7.3	Aircraft Installation	64
7.4	Check Point Residuals	66
7.5	Predicted Camera Orientation Accuracy	67
7.6	Variations in INS-Camera Orientation	68
7.7	INS Data Discontinuity	69
7.8	Variations in INS-Camera Orientation With Corrected Pitch	71

7.9	Roll Error in First Flight Line Due to a 5 ms Time Delay	72
7.10	INS Time Delay Estimation	73
7.11	x-Gyro and Accelerometer FFT, Lab Environment	75
7.12	x-Gyro and Accelerometer FFT, Aircraft Standing and Engines Running	75
7.13	y-Gyro FFT, Aircraft Standing and Engines Running	76
7.14	x-Gyro and Accelerometer FFT During the First Flight Line	77
7.15	z-Accelerometer FFT During the First Flight Line	77
7.16	Error in Roll Due to Aircraft Vibration on the Runway	78
7.17	Error in Pitch Due to in Flight Aircraft Vibrations	79

NOTATION

i) Conventions

- a) Matrices are upper case and bold
- b) Vectors are lower case and bold
- c) Rotation matrices between coordinate systems are defined by a subscript and a superscript denoting the two coordinate systems, (e.g. \mathbf{R}_b^e indicates a transformation from the body frame (b) to the earth-fixed frame (e)). The angular velocity vector, ω_{ib}^b , represents the rotation rate of the body frame with respect to the inertial frame expressed in the body frame.
- d) The following operators are defined as:
 - (+) Kalman update
 - (-) Kalman prediction
 - A^T matrix transpose
 - A^{-1} matrix inverse
 - $\dot{\mathbf{x}}$ time-derivative of vector
 - Δ single difference between receivers
 - $\hat{\mathbf{x}}$ estimated value
 - $\tilde{\mathbf{x}}$ measured value
 - x_0 initial value

ii) Coordinate Systems

Operational Inertial (i):

Approximate inertial frame of reference for INS measurements.

- origin: at centre of mass of the Earth
- x^i : towards the mean vernal equinox
- y^i : completes a right-handed system
- z^i : towards the mean celestial pole

Earth (e):

- origin: at centre of mass of the Earth
- x^e : towards the mean Greenwich meridian in the equatorial plane
- y^e : completes a right-handed system
- z^e : towards the mean celestial pole

The rotation of the earth-fixed frame with respect to the inertial frame is given by

$$\omega_{ie}^e = \begin{pmatrix} 0 \\ 0 \\ \omega_{\text{Earth}} \end{pmatrix} = \begin{pmatrix} 0 \\ 0 \\ 7.2921158 \text{ rad} \cdot \text{sec}^{-1} \end{pmatrix}$$

Local-level (l)

Refers to the chosen reference ellipsoid.

- origin: at the centre of the body frame
- x^l : towards ellipsoidal east

y^l : towards ellipsoidal north

z^l : upwards along ellipsoidal normal

The transformation matrix between the local-level frame and the earth-fixed frame is:

$$\mathbf{R}_l^e = \begin{pmatrix} -\sin \lambda & -\sin \phi \cos \lambda & \cos \phi \cos \lambda \\ \cos \lambda & -\sin \phi \sin \lambda & \cos \phi \sin \lambda \\ 0 & \cos \phi & \sin \phi \end{pmatrix}$$

where,

ϕ is the geodetic latitude

λ is the geodetic longitude

Body frame (b):

origin: at the centre of the INS accelerometer triad

x^b : towards the right side of the INS block seen from the front panel

y^b : opposite to the front panel, generally in forward direction

z^b : upwards and completing a right-handed system

The transformation matrix between body frame and local-level frame is:

$$\mathbf{R}_b^l = \begin{pmatrix} \cos \phi \cos \psi - \sin \theta \sin \phi \sin \psi & -\cos \theta \sin \psi & \sin \phi \cos \psi + \sin \theta \cos \phi \sin \psi \\ \cos \phi \sin \psi + \sin \theta \sin \phi \cos \psi & \cos \theta \cos \psi & \sin \phi \sin \psi - \sin \theta \cos \phi \cos \psi \\ -\cos \theta \sin \phi & \sin \theta & \cos \theta \cos \phi \end{pmatrix}$$

where,

θ, φ, ψ are three Euler angles defined as:

θ pitch, around x-axis, positive counter-clockwise when seen from the positive end of the axis

φ roll, around y-axis, positive counter-clockwise when seen from the positive end of the axis

ψ yaw, around z-axis, positive counter-clockwise when seen from the positive end of the axis

In navigation applications, the axes of the body frame often correspond to the vehicle axes (i.e. x^b - right side, y^b - forward, z^b - upward). This requires a rigorous alignment between the body axes defined here and the vehicle axes (right, forward, upward).

iii) Symbols

A	design matrix
α	azimuth
b	accelerometer bias
c	speed of light
C^e	Kalman measurement noise covariance matrix
C^w	Kalman filter process noise covariance matrix
C^x	Kalman state vector covariance matrix
d	gyro drift

dT	receiver clock error
dt	satellite clock error
f	specific force vector
F	specific force skew-symmetric matrix
ε	initial misalignment error
ϕ	geodetic latitude, rotation about y-axis between mapping and photo planes
Φ	carrier phase
$\dot{\Phi}$	phase rate
φ	roll
γ	normal gravity
h	geodetic height
I	identity matrix
K	Kalman gain matrix
κ	rotation about z-axis between mapping and photo planes
λ	geodetic longitude
M	meridian radius of curvature
M	rotation matrix from mapping plane to photo plane
N	prime vertical radius of curvature, carrier phase ambiguity
l	vector of measurements
Ω	three parameter skew-symmetric matrix
P	pseudorange

θ	pitch
\mathbf{Q}	spectral density matrix
\mathbf{r}	position vector
R_E	mean radius of the Earth
ρ	geometrical distance between receiver and satellite
\mathbf{v}	velocity vector
ω	angular rate, rotation about x-axis between mapping and photo planes
\mathbf{w}	process noise vector
ψ	yaw

CHAPTER 1

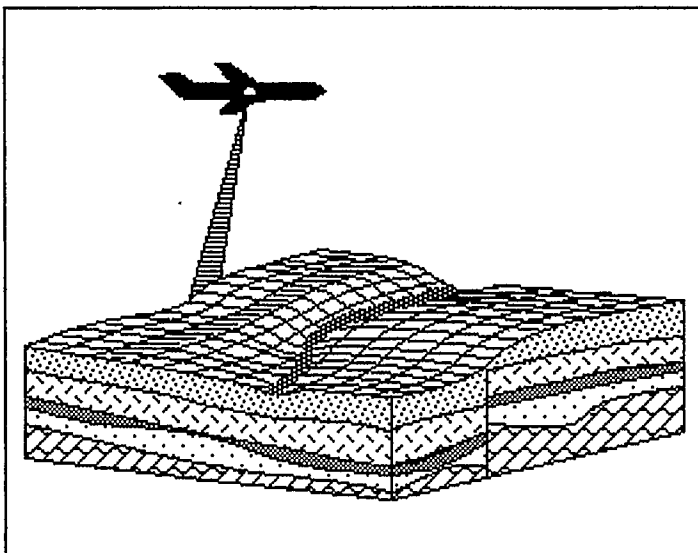
INTRODUCTION

1.1 Background and Objective

The integration of a strapdown Inertial Navigation System (INS) with receivers of the Global Positioning System (GPS) has been an area of intensive research over the last decade. Using such an integrated system, precise attitude and position of moving platforms can be obtained.

An on-board positioning and orientation system can be used for georeferencing of remotely sensed data, (see Figure 1.1). In other words, determining attitude and position of captured images with sufficient accuracy, allows their direct interpretation in object space. The emphasis in this

Figure 1.1 Image Georeferencing by On-Board Navigation Sensors



thesis will be on precise attitude determination or, more precisely, on the improvement of INS attitude by GPS updates.

The Global Positioning System, initially conceived by military groups for real-time navigation has been adapted for differential kinematic surveying by improving the positioning accuracies from several metres to subdecimetre level in post-mission mode (Remondi 1985, Mader 1989, Schwarz et al., 1989). By completing the full satellite constellation in 1993, GPS became a recognized surveying method with many potential applications. Since GPS measurements require line of sight between satellite and receiver, its limitation lies mainly in loss of lock due to physical obstructions. GPS can also be used for attitude determination by employing a configuration of several antennas. However, the accuracy of such derived orientation parameters is rather limited by antenna separation and receiver noise and cannot compete with those derived from precise INS, (see e.g. El-Mowafy et al., 1994).

The Inertial Navigation System, originally developed for aircraft navigation, is a self contained device providing relative orientation and position. If operated in unaided mode its accuracy degrades quickly due to time dependent systematic errors. The growth of systematic errors can be substantially reduced by updating the inertial system with external measurements. Specially developed measuring techniques such as Zero Velocity Update Measurements constrain the error accumulation and significantly improve the quality of navigation parameters (Wong 1988). However, such techniques cannot be applied in airborne

surveying applications where the need for frequent updates has to be satisfied by more accurate position or velocity. Currently, only GPS can fulfil such requirements in terms of precision, range and efficiency. Thus, aiding INS by GPS position and velocity updates reduces time-accumulated errors in the Inertial Navigation System and gives superior attitude and position accuracy during short and long time spans (Lapucha 1990 and Cannon 1991).

Differential GPS more or less determines the position accuracy of an integrated system, while the attitude performance is determined by the quality of the inertial sensors. The type of INS used has a major influence on the cost of the integrated system. Therefore, a good knowledge of system errors is required in designing a precise attitude/positioning system for variety of airborne applications.

The benefits of on-board navigation sensors for airborne remote sensing applications are substantial. Traditionally, in order to georeference images of aerial photogrammetry, six parameters of camera exterior orientation have to be found by correlation between ground control points and their corresponding images. To be able to resolve these parameters at least three ground control points have to be established for each block of images. However, a number of additional ground control points is usually required to control the error propagation. This represents a significant portion of the aerotriangulation budget. Moreover, this cost can be prohibitive for image georeferencing in remote areas. If the parameters of exterior orientation can be derived from simultaneously flown on-board sensors with

sufficient accuracy, the economic advantages are obvious. Furthermore, such methods allow the georeferencing of images in near real time (Schwarz et al. 1993).

In the case of pushbroom imagery, parameters of exterior orientation are required for each scan line. Here, the support of control points is not sufficient and several rather complicated solutions have been proposed to overcome this problem (Hofmann 1988), but none of them has been accepted in practice. Again, the solution can be supplied by a precise attitude/positioning system.

Table 1.1 displays the attitude accuracies required for different application areas, expressed as root mean square errors (RMS). It indicates, that except for precise engineering applications, which require orientation at the level of half an arc minute or better, the bulk of applications requires an accuracy 1-3 arc minutes or considerably less.

Table 1.1 Accuracy Requirements For Airborne Application

Application Area	Attitude (RMS)	Position (RMS)
Engineering, Cadastral Mapping	15" - 30"	0.05 - 0.1 m
Remote Sensing (Detailed)	1' - 3'	0.2 -1.0 m
Resource Mapping	10' - 20'	2 -5 m

Although consistency tests have proved the feasibility of differential GPS to fulfil the position requirements (Cannon et al. 1992), attempts to confirm the orientation accuracy of

an airborne INS/GPS have not been successful (see Cannon (1991) for some unexpected difficulties).

The main objective of this thesis is to optimize INS/GPS integration for precise attitude determination and to assess current INS/GPS attitude performance in flight. Different approaches are used to demonstrate the feasibility of this technology for airborne remote sensing applications. Initially, the potential of INS and INS/GPS is examined through error analysis and via computer simulation. Then, the orientation stability of an actual strapdown inertial system under high angular velocities is tested in a well-controlled lab environment. To assess the in-flight orientation accuracy of an INS/GPS system, an independent data stream of superior accuracy is needed. The principle of inverse photogrammetry is used in this case to provide a base for attitude comparison.

1.2 Outline

Chapter 2 describes the concept of strapdown inertial navigation as the primary device for attitude determination. The process of obtaining orientation parameters from fundamental observables is given. Also sensor errors are discussed and their propagation is formulated within the INS error state model.

Chapter 3 introduces the principle of GPS positioning by reviewing the observables and their relationship to the unknown navigation parameters. It also outlines the major error sources in GPS relative positioning.

Chapter 4 examines the error model for attitude determination using a strapdown INS and specifies error sources which can be controlled by GPS integration. Decentralized Kalman filtering is then described as an approach for realizing the INS/GPS integration.

In Chapter 5, computer simulations are used as a first approach to assess orientation performance of a GPS-aided inertial navigation system. Moreover, it investigates optimal integration parameters, when inertial sensors of different quality are used.

The stability of orientation sensors of an actual strapdown INS is described in Chapter 6. The system output under different angular velocities is analyzed in a well-controlled lab environment in order to verify its capability to follow aircraft orientation dynamics.

Chapter 7 focuses on evaluating INS/GPS orientation accuracy under actual flight conditions. The principle of inverse photogrammetry is illustrated as an independent method, providing superior accuracy for attitude comparison. A medium scale (1:10,000) photogrammetric test with INS/GPS sensors on board is described. Afterwards, the photogrammetric results are evaluated in terms of attitude accuracy and taken as reference values for those derived from a strapdown inertial navigation system with GPS aiding. Some discrepancies between

anticipated values from simulations and those derived from the airborne test are explained by analyzing the spectral characteristics of the inertial signal.

The main conclusions derived from this research as well as some recommendations for further development of an integrated INS/GPS system in support of airborne remote sensing are given in Chapter 8.

CHAPTER 2

STRAPDOWN INERTIAL NAVIGATION SYSTEMS (SINS)

2.1 Principle

The basic theory underlying inertial navigation is Newton's second law describing particle motion in a gravity field with respect to an inertial frame:

$$\mathbf{f}_i = \mathbf{a}_i - \mathbf{g}_i \quad (2.1)$$

where \mathbf{f} is the specific force, \mathbf{a} is the vehicle acceleration and \mathbf{g} stands for the gravity acceleration. By measuring the specific force, the vehicle acceleration can be extracted from Equation 2.1 assuming known gravity signal along the vehicle trajectory. Vehicle velocity can be obtained by integrating the acceleration with respect to time. Similarly, the relative position is acquired by velocity integration with respect to time.

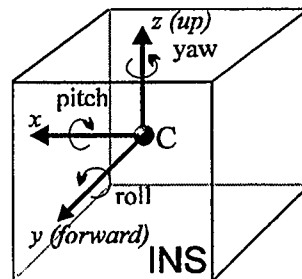
The INS senses all vehicle rotation rates and accelerations with respect to the inertial frame along a given trajectory. The accelerometer measurements are to be transformed from the inertial frame to the computation frame by a rotation matrix. The rotation matrix is calculated

from the angular velocity measurements and known rates between computation and inertial frames.

2.2 General Description

A strapdown Inertial Navigation System is composed of a triad of gyroscopes and a triad of accelerometers. The gyroscope triad senses the angular velocity of the platform with respect to inertial space and the accelerometer triad measures the specific force along the trajectory. The strapdown system is 'hard-mounted' to the vehicle and the sensor output axes coincide with the body frame. Figure 2.1 shows the body frame together with the definition of the three rotation angles: roll, pitch and yaw.

Figure 2.1 INS Body Frame



Since a strapdown INS does not have to feed back the actual navigation parameters for system stabilization and control, all raw angular rates and specific force measurements can be recorded and processed post mission.

The raw measurements can be mechanized in different coordinate systems (frames), such as the Earth-centered-Earth-fixed (ECEF) coordinate frame (Wei et al., 1990) or the local-level frame (Wong et al., 1983). Each implementation has different advantages and disadvantages. The local-level frame is commonly used because the output of conventional geographic coordinates and simple gravity modelling is convenient for many applications. However, the mechanization equations in this frame are rather complicated, especially when implemented with wander azimuth in order to avoid singularity at the poles. On the other hand, mechanization in the ECEF frame is simpler and the output in terms of geocentric Cartesian coordinates is optimal for integration with GPS. Disadvantages of this implementation are a more complicated normal gravity model and the additional transformation to geographic coordinates.

2.3 INS Mechanization in Earth-Centered-Earth-Fixed (ECEF) Frame

Wei and Schwarz (1990) indicate that the ECEF model implementation gives slightly better results and should be used for precise applications employing GPS/INS integration, especially when geocentric Cartesian coordinates are required. The fundamental set of differential equations that transforms inertial measurements to position, velocity and attitude in the Earth-fixed frame can be written in the following form (Wei et al. 1990).

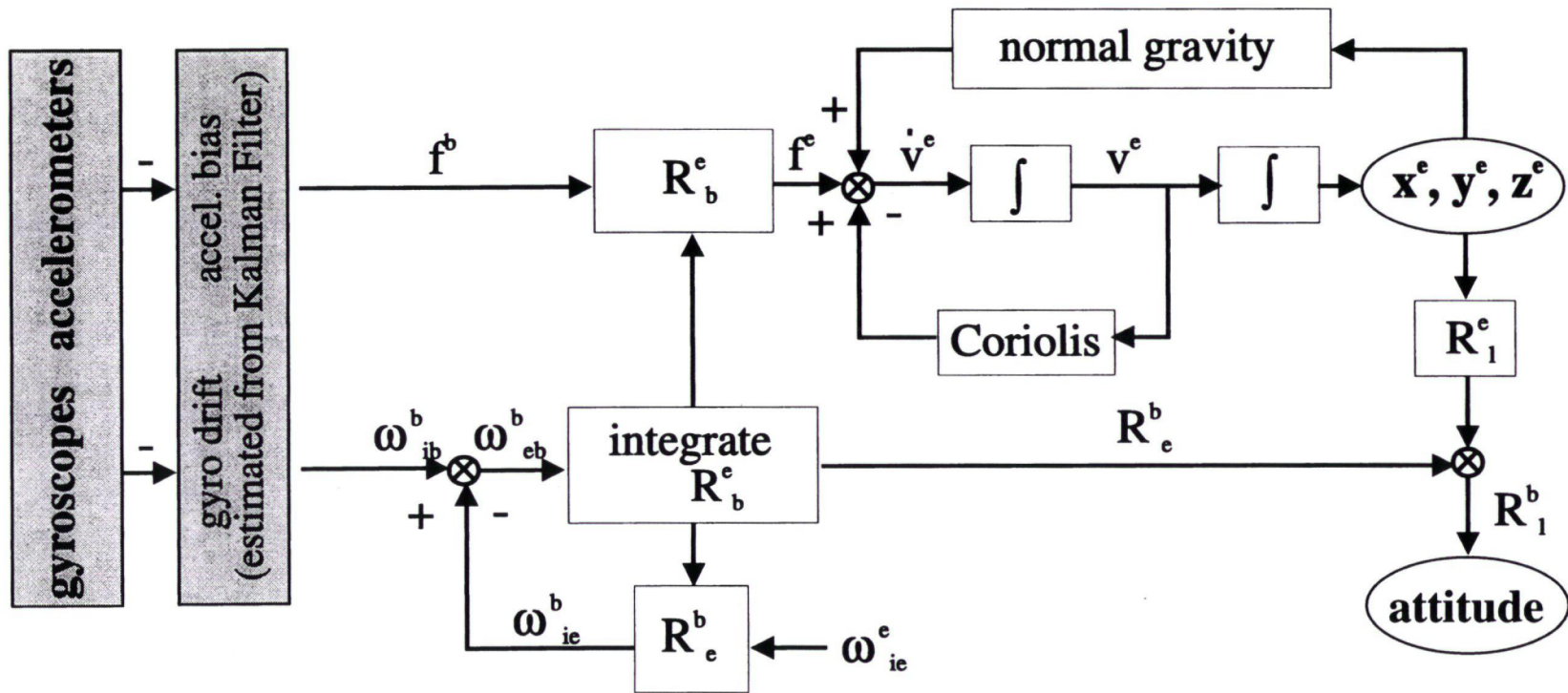
$$\begin{pmatrix} \dot{\mathbf{r}}^e \\ \dot{\mathbf{v}}^e \\ \dot{\mathbf{R}}_b^e \end{pmatrix} = \begin{pmatrix} \mathbf{v}^e \\ \mathbf{R}_b^e \mathbf{f}_b - 2\boldsymbol{\Omega}_{ie}^e \mathbf{v}^e + \boldsymbol{\gamma}^e \\ \mathbf{R}_b^e \boldsymbol{\Omega}_{eb}^b \end{pmatrix} \quad (2.2)$$

where

- \mathbf{r} is the position vector (m)
- \mathbf{v} is the velocity vector (m/s)
- \mathbf{f} is the specific force vector (m/s²)
- \mathbf{R}_b^e is the transformation matrix from body frame to Earth-fixed frame
- $\boldsymbol{\Omega}_{eb}^b$ is the skew-symmetric matrix of the angular velocity vector $\boldsymbol{\omega}_{eb}^b$ of the body frame with respect to the Earth-fixed frame
- $\boldsymbol{\Omega}_{ie}^e$ is the skew-symmetric matrix of the angular velocity vector $\boldsymbol{\omega}_{ie}^e$ of the Earth-fixed frame with respect to the inertial frame.

The algorithmic flowchart of the computation process is shown in Figure 2.1. Once the initial orientation is given, gyro measurement data are numerically integrated to obtain the transformation matrix between the inertial and computational frame (Equation 2.2, third part). The computed transformation matrix is then used to transform specific force measurements to the computation frame. After adding normal gravity and subtracting the Coriolis force from the specific force, acceleration of the vehicle is obtained which, after integration, provides velocity information (Equation 2.2). Position is derived by integrating velocity over time. The detailed computation formulas can be found in Schwarz and Wei (1994).

Figure 2.2 Inertial Mechanization Equations in Earth-Fixed Frame



2.4 Orientation from a Strapdown INS

The attitude, i.e. the inclination of three principal axes of the body frame with respect to the local-level frame, can be described by the rotation matrix \mathbf{R}_b^l , also called attitude matrix. The attitude matrix can be obtained from the matrix product of three elementary matrices describing consecutive rotations about the axes of the body frame. The angles of rotation are Euler angles, i.e. pitch(θ), roll(φ), yaw(ψ). Since the rotations around body frame axes are successive, the magnitude of roll, pitch and yaw is affected by the sequence of the rotation. The \mathbf{R}_b^l matrix has been defined as

$$\mathbf{R}_b^l = \left\{ \mathbf{R}_y(\varphi) \cdot \mathbf{R}_x(\theta) \cdot \mathbf{R}_z(\psi) \right\}^T \quad (2.3)$$

Euler angles of rotation can be computed from the elements of this matrix as

$$\begin{aligned} \theta &= \cos^{-1} \left(\mathbf{R}_b^l(3,2) \right) \\ \varphi &= \tan^{-1} \left(\frac{-\mathbf{R}_b^l(3,1)}{\mathbf{R}_b^l(3,3)} \right) \\ \psi &= \tan^{-1} \left(\frac{-\mathbf{R}_b^l(1,2)}{\mathbf{R}_b^l(2,2)} \right) \end{aligned} \quad (2.4)$$

The attitude matrix computation can be summarized by the following equation:

$$\mathbf{R}_1^b = \mathbf{R}_i^b \cdot \mathbf{R}_e^i \cdot \mathbf{R}_1^e \quad (2.5)$$

where \mathbf{R}_1^b is derived from the initial alignment and gyroscope outputs, \mathbf{R}_e^i is known since the Earth rotation rate is taken as a constant, and \mathbf{R}_1^e can be computed from the position on the reference ellipsoid.

The primary source of information for determining changes in attitude are gyroscopes. Accelerometers are mainly used for velocity and position determination and to obtain the initial orientation. If external information on position is not available, the INS derived position is used for updating the \mathbf{R}_1^e matrix.

2.5 Initial Alignment

An initial static alignment has to precede the survey in order to find the initial transformation matrix between body frame and local-level frame, i.e. the \mathbf{R}_b^l matrix. Once this relation is found, the \mathbf{R}_b^e matrix is obtained from the product $\mathbf{R}_b^l \cdot \mathbf{R}_l^e$. The initial alignment is done in two stages; coarse and fine alignment. The coarse alignment estimates the attitude parameters approximately. These are then refined in the fine alignment.

The coarse alignment procedure computes the pitch, roll and azimuth by the assumption that nothing but Earth rotation and gravity are sensed. In that case,

$$\omega_{ie}^l = \mathbf{R}_b^l \omega_{ie}^b = \begin{pmatrix} \omega_{ie} \sin \alpha \cos \phi \\ \omega_{ie} \cos \alpha \cos \phi \\ \omega_{ie} \sin \phi \end{pmatrix} \quad (2.6)$$

where ω_{ie} is the angular velocity of the Earth rotation, α is the azimuth, and ϕ is the geodetic latitude. The azimuth can be computed from the rotation rate sensed in the north and east directions, i.e.:

$$\alpha = \tan^{-1} \left(\frac{\omega_{ie, \text{north}}^l}{\omega_{ie, \text{east}}^l} \right) \quad (2.7)$$

and yaw is found as $\psi = -\alpha$. Pitch and roll angles are computed from the velocity in north (v^n) and east (v^e) directions, which is the velocity output of the mechanization equation after being transformed to the local-level frame

$$\phi = \sin^{-1} \left(\frac{v^n}{\gamma \Delta t} \right) \quad (2.8)$$

$$\theta = \sin^{-1} \left(\frac{v^e}{\gamma \Delta t} \right) \quad (2.9)$$

where γ is normal gravity, θ and φ are pitch and roll, respectively. The accuracy of the coarse alignment depends on the accuracy of the sensors; for the LTN-90-100 these errors are approximately 2 arc minutes for pitch and roll, and 1 degree in azimuth.

The fine alignment further refines the Euler angles together with pre-estimated gyro drifts and accelerometer biases using a Kalman filter algorithm. A 15 - state Kalman filter models the position errors, velocity errors and misalignment errors together with gyro drift and accelerometer bias. Zero velocity measurements are used every 10 seconds to update the filter. The fine alignment usually requires 10 to 20 minutes of stationary data. In laboratory conditions the achieved accuracy in the initial orientation after this time is about 2 arc minutes in azimuth and 30 arc second in pitch and roll (Liu 1992). However, this alignment accuracy can deteriorate in an unstable environment with differential movements or vibrations, as is often the case under field conditions.

2.6 INS Measurement Error Model

The strapdown INS output contains noise and systematic errors. The general model describing these errors can be found in Savage (1978). The specific model used here for simulation studies in Chapter 5 is adopted from Schwarz and Wei (1994).

2.6.1 Gyro Measurement Error Model

The ring-laser gyro output can be described as a combination of errorless angular velocity measurements and an error with the following characteristic:

$$\mathbf{d}\omega_{ib}^b = \mathbf{N}_\omega \omega_{ib}^b + \mathbf{S}_\omega \omega_{ib}^b + \mathbf{d}_\omega + \boldsymbol{\mu}_\omega + \boldsymbol{\delta}_\omega \quad (2.10)$$

where \mathbf{N}_ω is a skew-symmetric matrix describing non-orthogonality of the axes, \mathbf{S}_ω is a diagonal matrix of scale factor errors, \mathbf{d}_ω are gyro drifts, $\boldsymbol{\mu}_\omega$ contains random gyro drifts including correlated errors, random walk and white noise. $\boldsymbol{\delta}_\omega$ is noise due to dither and quantizer effects.

In terms of error characteristics, gyro drifts and gyro scale factor errors behave as random constants, gyro drift uncertainty can be modeled by a first-order Gauss-Markov process and random walk, dither and quantizer effect can be considered as a white noise. The non-orthogonality of the sensor axes can be determined via calibration.

2.6.2 Accelerometer Measurement Error Model

The error model for accelerometer measurements is given as:

$$\mathbf{d}\mathbf{f}^b = \mathbf{N}_f \mathbf{f}^b + \mathbf{S}_f \mathbf{f}^b + \mathbf{S}_2 \mathbf{F}^b \mathbf{f}^b + \mathbf{b}_f + \boldsymbol{\mu}_f + \boldsymbol{\delta}_f \quad (2.11)$$

where \mathbf{N}_f is a skew-symmetric matrix representing the non-orthogonality of the sensor axes, \mathbf{S}_f is the diagonal matrix of the scale factor errors, \mathbf{S}_2 is a matrix expressing second-order scale nonlinearity, \mathbf{b}_f is the accelerometer bias, μ_f represents random errors including correlated errors, random walk, and sensor white noise. δ_f is due to dither error and quantizer effect. The misalignment of the accelerometer axes is deterministic. Scale factor and scale factor nonlinearity act as random constants. Accelerometer sensor noise can be characterized by first-order Gauss-Markov processes and errors due to dither and quantizer can be considered as uncorrelated noise.

2.7 INS Error State Model

The INS sensor errors described in the previous paragraph cause a perturbation of the navigation quantities, e.g. the attitude. Some of these errors have to be estimated and subtracted from the raw sensor output prior to entering the navigation equation (Figure 2.1). Before applying an error estimation process, e.g. Kalman filtering, one has to develop an error model describing their rate of change. This can be represented by a set of linear differential equations of the form:

$$\dot{\mathbf{x}} = \mathbf{F} \mathbf{x} + \mathbf{w} \quad (2.12)$$

where \mathbf{x} is the error state vector, \mathbf{F} is the dynamics matrix and \mathbf{w} describes the system noise. In this case the sensor error states accommodate gyro drift and accelerometer bias. Other sensor errors, e.g. scale factor errors and misalignment, are treated as process noise. System

error states contain navigation parameters. Altogether, the 15 error state model in the Earth-fixed frame is given by:

$$\mathbf{x} = \{\delta x^e, \delta y^e, \delta z^e, \delta v_x^e, \delta v_y^e, \delta v_z^e, \delta \varepsilon_x^e, \delta \varepsilon_y^e, \delta \varepsilon_z^e, d_x^b, d_y^b, d_z^b, b_x^b, b_y^b, b_z^b\} \quad (2.13)$$

where

- $\delta x^e, \delta y^e, \delta z^e$ are three position errors in the Earth-fixed frame;
- $\delta v_x^e, \delta v_y^e, \delta v_z^e$ are three velocity errors in the Earth-fixed frame;
- $\delta \varepsilon_x^e, \delta \varepsilon_y^e, \delta \varepsilon_z^e$ are three misalignment errors in the Earth-fixed frame;
- $\delta d_x^b, \delta d_y^b, \delta d_z^b$ are three gyro drift errors in the body frame;
- $\delta b_x^b, \delta b_y^b, \delta b_z^b$ are three accelerometer biases in the body frame.

Equation (2.12) for this dynamic model can be expressed by (Schwarz and Wei 1994):

$$\begin{aligned} \begin{pmatrix} \delta \dot{v}_x^e \\ \delta \dot{v}_y^e \\ \delta \dot{v}_z^e \end{pmatrix} &= \begin{pmatrix} N_{11} & N_{12} & N_{13} \\ N_{21} & N_{22} & N_{23} \\ N_{31} & N_{32} & N_{33} \end{pmatrix} \begin{pmatrix} \delta x^e \\ \delta y^e \\ \delta z^e \end{pmatrix} + \begin{pmatrix} 0 & 2\omega_e & 0 \\ -2\omega_e & 0 & 0 \\ 0 & 0 & 0 \end{pmatrix} \begin{pmatrix} \delta v_x^e \\ \delta v_y^e \\ \delta v_z^e \end{pmatrix} \\ &+ \begin{pmatrix} 0 & f_z^e & -f_y^e \\ -f_z^e & 0 & f_x^e \\ f_y^e & -f_x^e & 0 \end{pmatrix} \begin{pmatrix} \varepsilon_x^e \\ \varepsilon_y^e \\ \varepsilon_z^e \end{pmatrix} + \begin{pmatrix} C_b^e(1,1) & C_b^e(1,2) & C_b^e(1,3) \\ C_b^e(2,1) & C_b^e(2,2) & C_b^e(2,3) \\ C_b^e(3,1) & C_b^e(3,2) & C_b^e(3,3) \end{pmatrix} \begin{pmatrix} b_x^b \\ b_y^b \\ b_z^b \end{pmatrix} + \begin{pmatrix} w_4 \\ w_5 \\ w_6 \end{pmatrix} \end{aligned} \quad (2.14)$$

$$\begin{pmatrix} \delta \dot{x}^e \\ \delta \dot{y}^e \\ \delta \dot{z}^e \end{pmatrix} = \begin{pmatrix} \delta v_x^e \\ \delta v_y^e \\ \delta v_z^e \end{pmatrix} \quad (2.15)$$

$$\begin{pmatrix} \dot{\varepsilon}_x^e \\ \dot{\varepsilon}_y^e \\ \dot{\varepsilon}_z^e \end{pmatrix} = \begin{pmatrix} 0 & \omega_e & 0 \\ -\omega_e & 0 & 0 \\ 0 & 0 & 0 \end{pmatrix} \begin{pmatrix} \varepsilon_x^e \\ \varepsilon_y^e \\ \varepsilon_z^e \end{pmatrix} + \begin{pmatrix} C_b^e(1,1) & C_b^e(1,2) & C_b^e(1,3) \\ C_b^e(2,1) & C_b^e(2,2) & C_b^e(2,3) \\ C_b^e(3,1) & C_b^e(3,2) & C_b^e(3,3) \end{pmatrix} \begin{pmatrix} d_x^b \\ d_y^b \\ d_z^b \end{pmatrix} + \begin{pmatrix} w_7 \\ w_8 \\ w_9 \end{pmatrix} \quad (2.16)$$

$$\begin{pmatrix} \delta \dot{d}_x^b \\ \delta \dot{d}_y^b \\ \delta \dot{d}_z^b \end{pmatrix} = \begin{pmatrix} w_{10} \\ w_{11} \\ w_{12} \end{pmatrix} \quad (2.17)$$

$$\begin{pmatrix} \delta \dot{b}_x^b \\ \delta \dot{b}_y^b \\ \delta \dot{b}_z^b \end{pmatrix} = \begin{pmatrix} w_{13} \\ w_{14} \\ w_{15} \end{pmatrix} \quad (2.18)$$

where w_1 to w_{15} denote process noise and f_x^e , f_y^e and f_z^e are specific force components in the Earth-fixed frame. N_{11} to N_{33} represent the influence of the normal gravity error. Detailed computations can be found in Wei and Schwarz (1990).

CHAPTER 3

THE GLOBAL POSITIONING SYSTEM (GPS)

This chapter gives a brief introduction to GPS methodology by reviewing its concept, observables and their relationship to the unknown parameters. It also outlines the major error sources in GPS relative positioning.

3.1 General Description

The Global Positioning System (GPS) is a satellite-based radio positioning system developed by the U.S. Department of Defence and designed for navigation. It includes three major segments - the satellite segment, the control segment and the user segment.

The Satellite segment consists of 24 satellites orbiting around the Earth in six orbital planes inclined at 55 degrees. Every orbital plane consists of four, evenly distributed satellites orbiting 20 000 km above the Earth surface. The satellites are continuously transmitting a navigation message containing information about the satellite clock, the orbital parameters and the satellite health. The navigation message is transmitted on two frequencies, 1575.42

and 1227.60 Mhz, called L1 and L2, respectively. Both frequencies are modulated by pseudo random precise (P) code being transmitted at 10.23 Mhz with a repetition time of 267 days. Furthermore, L1 is also modulated by the coarse acquisition (C/A) code which is duplicated every millisecond on the frequency of 1.023 Mhz.

The control segment is composed of five monitoring stations that perform continuous satellite tracking and one master control station which collects these data to recompute the orbit and satellite clock parameters. This updated information is then uploaded to the satellites.

The user segment consists of GPS receivers which receive the radio signal from the visible satellites and computes the navigation solution using the navigation message.

3.2 Observation Equations

In principle, there are three different observables available on both GPS frequencies, namely, pseudorange, carrier phase and phase rate. It should be noted, however, that not all receivers output each type of measurement.

The pseudorange observable is measured by comparing the received code with its replica generated by the receiver. This comparison provides the time shift between two signals. Multiplying this time difference by the speed of light yields the distances between the receiver and satellite in the following form:

$$\rho = \sqrt{(x_s - x_r)^2 + (y_s - y_r)^2 + (z_s - z_r)^2} \quad (3.1)$$

where x, y, z are three dimensional coordinates. The subscript s denotes satellite coordinates computed from broadcasted ephemeris and the subscript r represents the unknown receiver coordinates.

The carrier phase observables are made on a differential signal (beat signal) between receiver generated and Doppler shifted carrier coming from the satellite. The fractional part of one cycle is measured and the change of cycles is counted as a integer number. The initial uncertainty in the number of cycles, the so-called phase ambiguity, has to be solved in order to gain information from precise carrier phase measurements. A sudden change in ambiguity number due to atmospheric, dynamic or physical signal disturbance is called a cycle slip.

The phase rate observable are performed by determining the Doppler frequency changes of the incoming signal caused by the relative motion between the receiver and satellite. This information is used for velocity determination and can be computed as

$$\dot{\Phi} = \frac{(x_s - x_r)(\dot{x}_s - \dot{x}_r) + (y_s - y_r)(\dot{y}_s - \dot{y}_r) + (z_s - z_r)(\dot{z}_s - \dot{z}_r)}{\sqrt{(x_s - x_r)^2 + (y_s - y_r)^2 + (z_s - z_r)^2}} \quad (3.2)$$

The observation equations for all three types of measurements are

$$\begin{aligned} P &= \rho + c(dt - dT) + d_{\text{ion}} + d_{\text{trop}} + d_{\rho} + e_p \\ \Phi &= \rho + c(dt - dT) + \lambda N - d_{\text{ion}} + d_{\text{trop}} + d_{\rho} + e_{\Phi} \\ \dot{\Phi} &= \dot{\rho} + c(\dot{dt} - \dot{dT}) - \dot{d}_{\text{ion}} + \dot{d}_{\text{trop}} + \dot{d}_{\rho} + \dot{e}_{\Phi} \end{aligned} \quad (3.3)$$

where P is the pseudorange observation (m)

Φ is the carrier phase observation (m)

$\dot{\Phi}$ is the phase rate (Doppler) observation

ρ is the true receiver-satellite range (m)

c is the speed of light (m/s)

dt is the satellite clock error (s)

dT is the receiver clock error (s)

N is the carrier phase initial ambiguity (integer number of cycles)

λ is the carrier phase wave length (m/cycle)

d_{ion} is the correction due to ionospheric delay (m)

d_{trop} is the correction due to tropospheric delay (m)

$e_{p,\Phi}$ is the measurement noise including multipath (m)

($\dot{\cdot}$) denotes the time derivative.

3.3 Differential Observation and Residual Errors

Some of the error sources in Equation (3.3) can be eliminated or substantially reduced by using differential observations. This is achieved by subtracting satellite observations at monitoring (master) stations of known position from simultaneously collected data at the remote station. Such a method is called single differencing and eliminates the satellite clock error. Further error reduction and elimination of receiver clock errors is achieved by double differencing, i.e. differencing two single differences across two satellites.

The observation equations in double differencing are given by

$$\begin{aligned}
 \nabla\Delta P &= \nabla\Delta \rho + \nabla\Delta d_{\text{ion}} + \nabla\Delta d_{\text{trop}} + e\nabla\Delta_p \\
 \nabla\Delta \Phi &= \nabla\Delta \rho + \lambda \cdot \nabla\Delta N - \nabla\Delta d_{\text{ion}} + \nabla\Delta d_{\text{trop}} + e\nabla\Delta_\Phi \\
 \nabla\Delta \dot{\Phi} &= \nabla\Delta \dot{\rho} + \nabla\Delta \dot{d}_{\text{ion}} + \nabla\Delta \dot{d}_{\text{trop}} + \dot{e}\nabla\Delta_\dot{\Phi}
 \end{aligned} \tag{3.4}$$

where $\nabla\Delta$ represents the double differencing of the corresponding value.

The residual orbital, tropospheric and ionospheric errors are functions of the separation between the monitor and remote receivers. Assuming correct ambiguity values, the position accuracy computed from phase observation is somewhere between 3 - 6 ppm (Mader and Lucas, 1989). This implies subdecimetre accuracy for 15 km receiver separation. Within this range, the velocity error remains within the magnitude of few centimetres per second (Cannon et al. 1992).

3.4 GPS Error State Model

To obtain a continuous trajectory from discrete observations, the GPS error model assumes either constant acceleration or, as it is in this case, constant velocity between measurements (Schwarz et al., 1989). The GPS state error vector can be expressed simply in terms of position and velocity as

$$\mathbf{x} = \{\delta x^e, \delta y^e, \delta z^e, \delta v_x^e, \delta v_y^e, \delta v_z^e\} \quad (3.5)$$

with the dynamic model given as

$$\begin{pmatrix} \delta \dot{x}^e \\ \delta \dot{y}^e \\ \delta \dot{z}^e \end{pmatrix} = \begin{pmatrix} \delta v_x^e \\ \delta v_y^e \\ \delta v_z^e \end{pmatrix} \quad (3.6)$$

$$\begin{pmatrix} \delta \dot{v}_x^e \\ \delta \dot{v}_y^e \\ \delta \dot{v}_z^e \end{pmatrix} = \begin{pmatrix} w_4 \\ w_5 \\ w_6 \end{pmatrix}$$

where w_4, w_5, w_6 is the process noise taking into account the disturbing accelerations.

In cases where carrier integer ambiguities are not determined prior to the kinematic survey or become unknown due to cycle slips or loss of lock, the state vector has to be augmented in the following way

$$\mathbf{x} = \{\delta x^e, \delta y^e, \delta z^e, \delta v_x^e, \delta v_y^e, \delta v_z^e, \delta N_1, \dots, \delta N_i\} \quad (3.7)$$

where δN is an integer correction to a satellite's new carrier phase ambiguity and i is the number of satellites. However, this change of the state vector may lead to substantial accuracy degradation.

CHAPTER 4

THE ERROR MODEL OF INS/GPS INTEGRATION FOR PRECISE ATTITUDE DETERMINATION

The strapdown INS as a primary device for attitude determination and the GPS have been described in the previous chapters. This chapter will inspect the error model for attitude determination and show that some of the systematic errors can be eliminated or reduced by using GPS position and velocity to update the INS. Then Kalman filtering will be introduced as an approach for realizing such integration. Afterwards, the concept of integration by a decentralized filtering is presented and important aspects of this process are mentioned.

4.1 Attitude Error Model Analysis

The essential features of the attitude error model will be examined in this section. The dynamic model for misalignment errors in the Earth-fixed frame is given by Equation (2.16). Since the GPS derived position and velocity will be used to update the INS, the orientation errors due to imperfect synchronization between the two measurement systems will be added to Equation (2.16) which can be rewritten in vector form as

$$\dot{\boldsymbol{\varepsilon}}^e = -\boldsymbol{\Omega}_{ie}^e \boldsymbol{\varepsilon}^e + \mathbf{R}_b^e \mathbf{d} + \dot{\mathbf{R}}_b^e d\mathbf{T} \quad (4.1)$$

where $\dot{\mathbf{R}}_b^1$ is the time derivative of the \mathbf{R}_b^1 matrix and $d\mathbf{T}$ is a synchronization error. Since attitude is related to the system of geodetic coordinates, Equation (4.1) is transformed to the local-level frame (Schwarz and Wei 1994)

$$\dot{\boldsymbol{\varepsilon}}^1 = -\delta \boldsymbol{\omega}_{il}^1 - \boldsymbol{\Omega}_{il}^1 \boldsymbol{\varepsilon}^1 + \mathbf{R}_b^1 \mathbf{d} + \dot{\mathbf{R}}_b^1 d\mathbf{T} \quad (4.2)$$

where the term $\boldsymbol{\Omega}_{ie}^1 \boldsymbol{\varepsilon}^1$ represents the effect due to initial misalignment, the term $\mathbf{R}_b^1 \mathbf{d}$ includes errors due to gyro noise, namely drift and white noise. The term $\delta \boldsymbol{\omega}_{il}^1$ represents errors in angular velocity due to the misorientation of the local-level frame as a result of position and velocity errors. This relationship is expressed by (Schwarz and Wei 1994)

$$\begin{pmatrix} \delta \omega_{il}^e \\ \delta \omega_{il}^n \\ \delta \omega_{il}^z \end{pmatrix} = \begin{pmatrix} 0 & 0 & \dot{\phi}/(M+h) \\ -\omega_e \sin \phi & 0 & -\dot{\lambda} \cos \phi/(N+h) \\ \omega_e \cos \phi + \dot{\lambda}/\cos \phi & 0 & -\dot{\lambda} \sin \phi/(N+h) \end{pmatrix} \begin{pmatrix} \delta \phi \\ \delta \lambda \\ \delta h \end{pmatrix} + \begin{pmatrix} 0 & -1/(M+h) & 0 \\ 1/(N+h) & 0 & 0 \\ \tan \phi/(N+h) & 0 & 0 \end{pmatrix} \begin{pmatrix} \delta v_e \\ \delta v_n \\ \delta v_z \end{pmatrix} \quad (4.3)$$

The transition matrix for a somewhat simplified error model of a local-level inertial system (Farrell 1976) contains the terms $\cos(\omega_s t)$ and $\sin(\omega_s t)/\text{const.}$, where $\omega_s = \sqrt{(g/R_E)}$ symbolizes the Schuler frequency. The Schuler frequency is the dominant error effect of the stand-alone local-level inertial system. Its period is about 84 minutes and its amplitude is a function of the initial misalignment and sensor errors (Britting 1971). However, if the velocity and position are given by GPS with sufficient accuracy, the term $\delta \omega_i^1$ in Equation (4.2) can be neglected which prevents the Schuler type errors from developing. The double difference GPS position and velocity provide sufficient accuracy (see Section 3.3) to keep attitude errors due to position and velocity errors below one tenth of an arc-second. Thus the significant errors affecting airborne attitude can be written as

$$\dot{\varepsilon}^1 = -\Omega_{ii}^1 \varepsilon^1 + \mathbf{R}_b^1 \mathbf{d} + \dot{\mathbf{R}}_b^1 \mathbf{dT} \quad (4.3)$$

The solution of Equation (4.3) can be written in general form as

$$\varepsilon^1 = \Phi(t, t_0) \Omega_{ii}^1 \varepsilon_0 + \int_{t_0}^t \Phi(t, \tau) \mathbf{R}_b^1 \mathbf{d}(\tau) + \int_{t_0}^t \Phi(t, \tau) \dot{\mathbf{R}}_b^1 \mathbf{dT} \cdot d\tau \quad (4.5)$$

where $\Phi(t, t_0)$ is transition matrix of a system of differential equation for the local-level inertial navigator (Britting 1971, Schwarz and Wei 1994); the first term of Equation (4.5) represents errors due to initial misalignment and the second term denotes integrated gyro errors as given by Equation (2.10).

In the following, the time dependent structure of the two terms in Equation (4.5) will be further analyzed and the influence of GPS updates on remaining attitude error sources will be investigated. Since it is difficult to analytically express the transition matrix with variable elements, some simplification will be introduced in the subsequent discussion. First by, considering the coefficient matrix as having constant elements, the transition matrix can be written as $\Phi(t, t_0) = \Phi(t - t_0)$. Second, the term \mathbf{R}_b^1 in Equation (4.3) will be neglected and the analytical form of the transition matrix is found by use of the inverse Laplace transform

$$\Phi(t - t_0) = \mathbf{L}^{-1}\left\{(\mathbf{sI} - \mathbf{\Omega}_B^1)^{-1}\right\} \quad (4.6)$$

as

$$\Phi_e(t) = \left[\frac{\omega_e \omega_n + \omega_e \omega_z}{\omega^2} + \frac{\omega^2 - \omega_e^2 - \omega_e \omega_n - \omega_e \omega_z}{\omega^2} \cos \omega t + (\omega_z - \omega_n) \sin \omega t \right] \quad (4.7)$$

where Φ_e is the transition matrix for the east channel, ω is the magnitude of angular velocity and ω_e , ω_n , ω_z represent its east, north and up components respectively. The transition matrices for the north channel is of a similar form.

Considering the same misalignment errors in east, north and up directions, the equation for attitude errors due to an initial misalignment in the east channel is given by

$$\boldsymbol{\varepsilon}_e^m = \left[\frac{\omega_e \omega_n + \omega_e \omega_z}{\omega^2} + \frac{\omega^2 - \omega_e^2 - \omega_e \omega_n - \omega_e \omega_z}{\omega^2} \cos \omega t + (\omega_z - \omega_n) \sin \omega t \right] \boldsymbol{\varepsilon}_0 \quad (4.8)$$

From the structure of the Equation (4.8) it can be concluded that initial misalignment errors show periodic behaviour and thus are bounded.

In order to analyze the second term in Equation (4.5), the gyro measurement model given by Equation (2.10) is simplified to a sum of constant gyro drift and random noise. Applying the simplified form of the transition matrix in Equation (4.7) to the second term in Equation (4.6) and considering only constant gyro drift, the attitude error due to constant gyro bias can be derived as

$$\boldsymbol{\varepsilon}_e^d = \left[\frac{\omega_e \omega_n + \omega_e \omega_z}{\omega^2} t + \frac{\omega^2 - \omega_e^2 - \omega_e \omega_n - \omega_e \omega_z}{\omega^2} \sin \omega t - (\omega_z - \omega_n) \cos \omega t \right] \mathbf{d}_c \quad (4.9)$$

Equation (4.9) implies that the attitude error due to constant gyro drift has a linear as well as periodic function and, therefore, is not bounded.

Furthermore, only the uncorrelated part of the random noise will be considered. The variance of the attitude errors for the east channel due to white noise can be expressed as

$$\sigma_e^2 = \int_{t_0}^t \int_{t_0}^t \Phi_t(t-\tau) E(d_w(\tau) d_w(\tau)) \Phi_t(t-\tau) d\tau d\tau \quad (4.10)$$

and after substituting the transition matrix in Equation (4.7) it becomes

$$\sigma_{\varepsilon_e}^2 = \mathbf{Q}_w \left[\frac{2A+D}{2\omega^4} t + \frac{2B}{\omega^5} \sin \omega t - \frac{2C}{\omega^5} \cos \omega t + \frac{D}{4\omega^5} \sin 2\omega t - \frac{E}{2\omega^5} \cos 2\omega t \right] \quad (4.11)$$

where

$$A = (\omega_e \omega_n + \omega_e \omega_z)^2;$$

$$B = (\omega_e \omega_n + \omega_e \omega_z) (\omega^2 - \omega_e^2 - \omega - \omega_e \omega_n - \omega_e \omega_z);$$

$$C = \omega_e (\omega_z^2 + \omega_n^2);$$

$$D = (\omega^2 - \omega_e^2 - \omega_e \omega_n - \omega_e \omega_z)^2;$$

$$E = (\omega^2 - \omega_e^2 - \omega_e \omega_n - \omega_e \omega_z) (\omega_z - \omega_n);$$

\mathbf{Q}_w is the spectral density matrix for white noise d_w .

The first term in the Equation (4.11) implies that gyro random errors cause divergence in INS attitude.

So far, it has been shown that attitude diverges due to gyro errors, namely gyro drift and random noise. Moreover, the initial misorientation generates an attitude oscillation with

frequency ω . These types of attitude errors can be reduced by GPS integration. This subject will be discussed in Section 4.3.

4.2 Kalman Filtering

The discrete Kalman filtering algorithm will be used for integrating measurements from the INS and GPS data streams in order to minimize the INS orientation error. Since its derivation is well documented in literature (Gelb 1974), only essential formulas for dynamic and measurement models are summarized in the following paragraphs.

The linear dynamic model in discrete form can be expressed as a solution of a set of first-order differential equations $\dot{\mathbf{x}} = \mathbf{F} \mathbf{x} + \mathbf{w}$ (Equation 2.12) as follows:

$$\mathbf{x}_k = \Phi_{k-1} \mathbf{x}_{k-1} + \mathbf{w}_{k-1} \quad (4.12)$$

where \mathbf{x} is the state vector, \mathbf{w} is the process noise and Φ is the transition matrix describing the change of the state vector between instances $k-1$ and k . For a linear model the transition matrix can be computed as

$$\Phi_{k-1} = e^{-\mathbf{F}\Delta t} = \mathbf{I} + \mathbf{F}\Delta t + \frac{(\mathbf{F}\Delta t)^2}{2!} + \dots \quad (4.13)$$

In many cases, this equation can be truncated after the first term.

The measurement model can be written as

$$\mathbf{l}_k = \mathbf{A}_k \mathbf{x}_k + \mathbf{v}_k \quad (4.14)$$

where \mathbf{l} is the measurement vector, \mathbf{A} is the design matrix and \mathbf{v} is the measurement noise.

The Kalman filter predicts the estimates from the instance $k-1$ for the instance k as

$$\hat{\mathbf{x}}_k(-) = \Phi_{k-1} \hat{\mathbf{x}}_{k-1}(+) \quad (4.15)$$

$$\mathbf{C}^{\mathbf{x}}(-) = \Phi_{k-1} \mathbf{C}_{k-1}^{\mathbf{x}}(+) \Phi_{k-1}^T + \mathbf{C}_{k-1}^{\mathbf{w}} \quad (4.16)$$

where $\hat{\mathbf{x}}$ represents the estimate of \mathbf{x} , $\mathbf{C}^{\mathbf{x}}$ and $\mathbf{C}^{\mathbf{w}}$ are the system and process noise covariance matrixes, $(-)$ symbolize predicted values and $(+)$ refers to values after measurements update.

The measurements are updating this prediction to obtain the best linear estimate of the system states as

$$\hat{\mathbf{x}}_k(+) = \hat{\mathbf{x}}_k(-) + \mathbf{K}_k [\mathbf{l}_k - \mathbf{A}_k \hat{\mathbf{x}}_k(-)] \quad (4.17)$$

$$\mathbf{C}_k^{\mathbf{x}}(+) = [\mathbf{I} - \mathbf{K}_k \mathbf{A}_k] \mathbf{C}_k^{\mathbf{x}}(-) \quad (4.18)$$

$$\mathbf{K}_k = \mathbf{C}_k^{\mathbf{x}}(-) \mathbf{A}_k^T [\mathbf{A}_k \mathbf{C}_k^{\mathbf{x}}(-) \mathbf{A}_k^T + \mathbf{C}_k^{\mathbf{e}}]^{-1} \quad (4.19)$$

where $\mathbf{C}^{\mathbf{e}}$ is covariance matrix of the measurement noise and \mathbf{K} is the Kalman gain matrix.

The Kalman filter operates under the assumption that the mean value of the processing noise and the measurement noise, as well as the correlation between them are zero. The covariance matrices are defined as

$$E[(\mathbf{x} - \hat{\mathbf{x}})(\mathbf{x} - \hat{\mathbf{x}})^T] = \mathbf{C}^x \quad (4.20)$$

$$E[\mathbf{w}_k \mathbf{w}_j^T] = \mathbf{C}^w \delta_{kj} \quad (4.21)$$

$$E[\mathbf{v}_k \mathbf{v}_j^T] = \mathbf{C}^e \delta_{kj} \quad (4.22)$$

where δ_{kj} is the Kronecker delta.

4.3 Estimation of INS Attitude Errors by GPS Aiding

This paragraph will discuss the principle of attitude error estimation via the discrepancy between the INS and GPS velocities. The essential characteristics of this principle can be found in the INS velocity error states (Equation 2.15) which can be written in vector form as

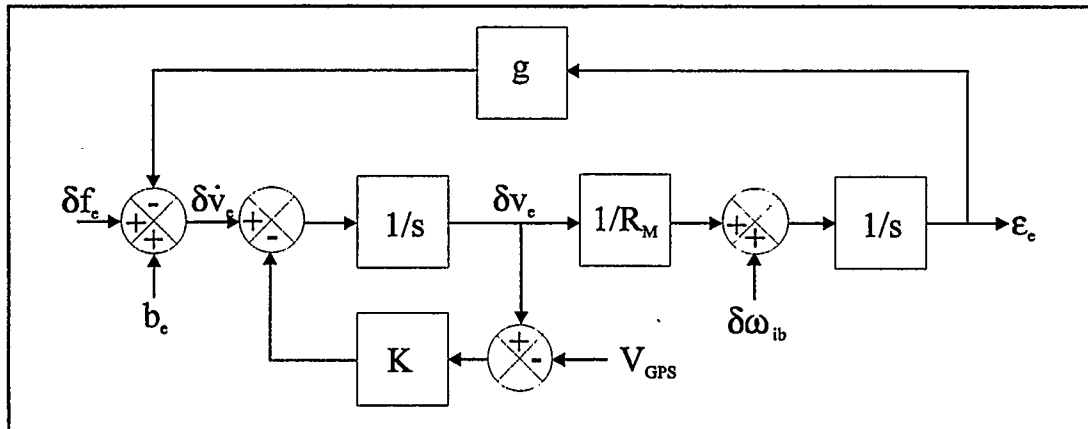
$$\delta \dot{\mathbf{v}}^e = \mathbf{N}^e \delta \mathbf{r}^e - 2\mathbf{\Omega}_{ie}^e \delta \mathbf{v}^e - \mathbf{F}^e \boldsymbol{\varepsilon}^e + \mathbf{R}_b^e \mathbf{b}^b \quad (4.23)$$

The terms due to $\delta \mathbf{v}$ and $\delta \mathbf{r}$ in Equation (4.23) are small and random when updating INS by GPS position and velocity. Thus, INS velocity errors can be expressed as a function of the misalignment errors and accelerometer biases as

$$\delta \dot{\mathbf{v}}^e = -\mathbf{F}^e \boldsymbol{\varepsilon}^e + \mathbf{R}_b^e \mathbf{b}^b \quad (4.24)$$

This relation suggests that, by feeding back corrected velocity measurements to the INS mechanization equation (Figure 2.1), the orientation error is reduced. The principle of damping the attitude error propagation with GPS velocity update is depicted for one channel in Figure 4.1.

Figure 4.1 INS East Channel With GPS Velocity Aiding



In Figure 4.1, \mathbf{K} represents the Kalman gain matrix or, in other words, the ratio between the estimated signal accuracy and the measurement noise. Once this ratio is determined from the covariance matrix propagation (Equation 4.19), \mathbf{K} is used to update the error state in Equation (4.17) as

$$\hat{\mathbf{x}}_k(+)=\hat{\mathbf{x}}_k(-)+\mathbf{K}_k\left[\mathbf{I}_k-\mathbf{A}_k\right] \hat{\mathbf{x}}_k(-) \quad (4.25)$$

where I_k represents the measurement and $A_k x_k$ the measurement prediction.

Using Figure 4.1, the Laplace transform of the attitude error is given by

$$\Phi(s) = \frac{s + k}{s^2 + ks + \omega_s^2} \quad (4.26)$$

Following Schwarz and Wei (1995), the transition matrix of the attitude error found as inverse Laplace transform of Equation (4.26) can be expressed by

$$\Phi(t) = e^{-\frac{k}{2}t} \left[\cos \omega_s t + \frac{k}{2\omega_s} \sin \omega_s t \right] \quad (4.27)$$

where $\omega_s = \sqrt{\omega_s^2 + k^2}$ is a modified Schuler frequency.

The principle described above also implies that orientation errors due to initial misalignment, gyro bias and noise can be estimated via INS/GPS integration. By using Equations (4.5) and (4.27) the attitude error is dampened with a scale coefficient of $e^{-\frac{k}{2}t}$. The accuracy of the estimation is strongly affected by the sensitivity of velocity errors to attitude errors. To illustrate this problem more specifically, Equation (4.24) will be transformed to the local-level frame and written in detail as

$$\begin{aligned}
\delta \dot{v}_e &= f_z \varepsilon_n - f_n \varepsilon_z + b_e \\
\delta \dot{v}_n &= -f_z \varepsilon_e + f_e \varepsilon_z + b_n \\
\delta \dot{v}_z &= f_n \varepsilon_e - f_e \varepsilon_n + b_z
\end{aligned} \tag{4.28}$$

where the subscripts e, n, z denote east, north and up components, f is the specific force measurement, ε is the misalignment error and b is the accelerometer bias. Equation (4.28) indicates that the velocity error in a particular channel is generated by misalignment errors coupled with specific force measurements in the other two channels. Since f_z is always of a large magnitude due to gravity, ε_e and ε_n can be observed continuously. In contrast, f_e and f_n have nonzero values only when the vehicle is accelerating in the horizontal plane. Thus, the accuracy of determining ε_z mainly depends on the extent of these manoeuvres. On the other hand, the tilt error determination is mainly limited by its correlation with the horizontal accelerometer bias (see Equation 4.28 and Figure 4.1).

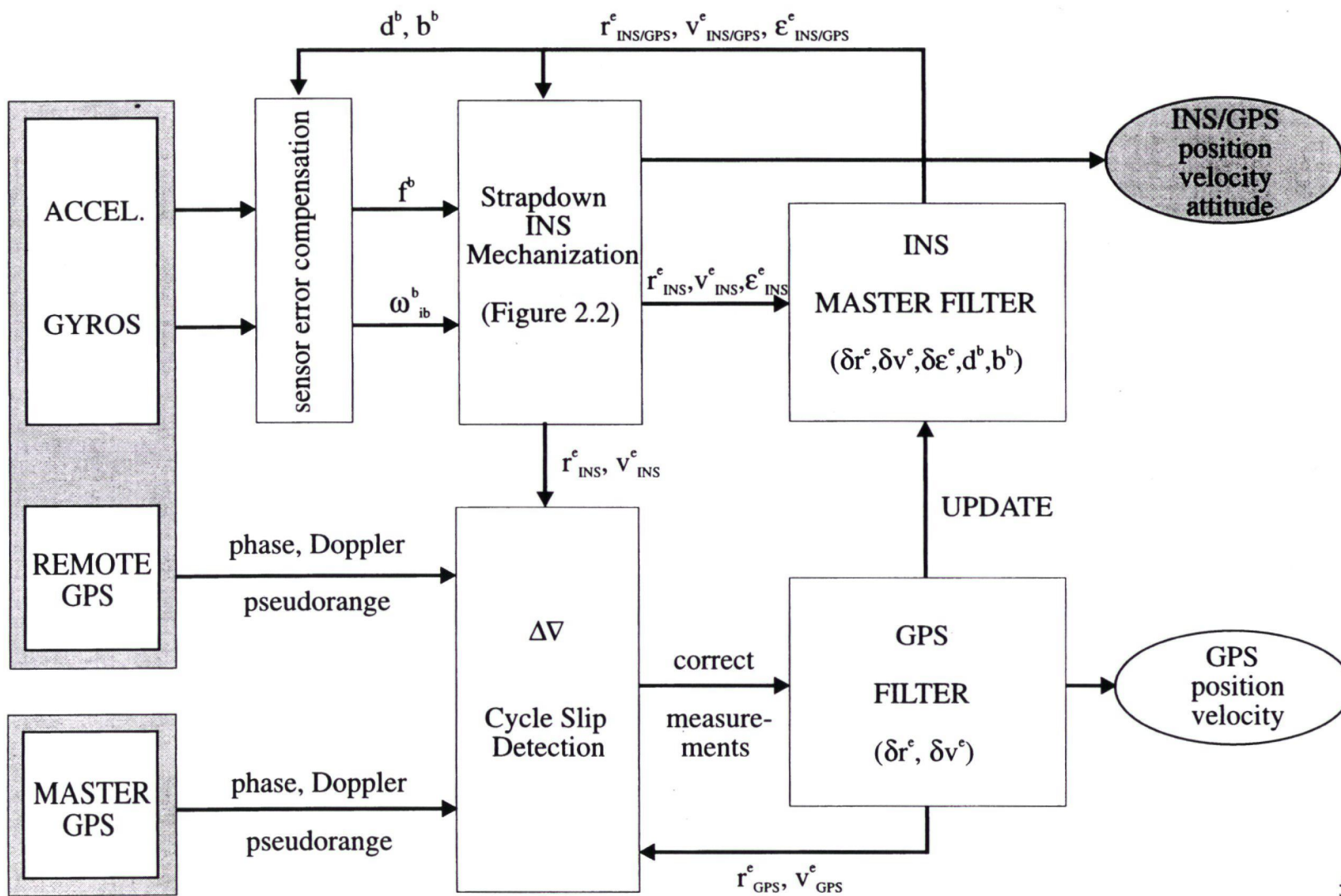
Generally, we can expect better accuracy in roll and pitch determination due to their strong correlation with the gravitational acceleration. The error in azimuth is usually observable indirectly through the horizontal velocity error which takes a longer time to develop. Furthermore, its determination is limited not only by horizontal accelerometer biases, but also by constant gyro biases.

4.4 INS/GPS Integration Strategies For Precise Attitude Determination

The actual implementation of the preceding theory for INS/GPS integration can use either centralized or decentralized Kalman filtering. Each concept has its advantages and disadvantages, but numerical results have not shown a significant difference between both designs (Wei et al. 1990). Since modification of existing INS/GPS software used for actual data processing employs the concept of decentralized filtering, only this method will be described in detail.

As shown in Figure 4.2, the decentralized Kalman filter configuration for an INS/GPS integration runs two filters in parallel. The GPS state vector is given by Equation (3.5) while the INS state vector is described by Equation (2.13). The GPS filter runs independently from the INS filter and its output is used to update the INS error states. The double difference pseudorange, carrier phase and phase rate observations form the measurement vector in the GPS filter. Its output (i.e. position and velocity) represents additional measurements which are used to update the INS master filter. The noise in these 'pseudo-measurements' is determined by the GPS filter covariance matrix. Updated error states in the INS master filter are fed back to correct INS raw measurements and the strapdown mechanization. Thus, the output from the mechanization contains INS/GPS integrated position, velocity and attitude information. This information is used to check the validity of GPS measurements and to help to resolve carrier phase ambiguity when a number of cycle slips or serious loss of lock occur in GPS measurements. The performance of the Kalman filter is sensitive to the correctness

Figure 4.2 Block Diagram of INS/GPS Integration



of the information contained in the covariance matrices. The initial covariances have to reflect the likely magnitude of specific parameters, otherwise the filter could diverge. The initial covariances of inertial sensors are determined from their statistics and the position and velocity covariances represent the accuracy of the initial data. The initial attitude covariance is determined during the alignment procedure.

The error analysis described in this chapter indicated that INS-derived attitude can benefit from frequent GPS updates in terms of reducing the systematic errors. However, since the characteristics of GPS position and velocity errors could introduce additional noise in INS/GPS attitude, optimal update intervals need to be investigated. This problem will be closely examined by means of simulation studies in Chapter 5.

After being integrated with GPS, the error structure of INS orientation errors is expected to have mainly random behaviour. Since these errors can be strongly correlated with actual hardware (synchronization) and its environment (aircraft vibrations), it is difficult to predict their magnitude. This will be the subject of investigation in Chapters 6 and 7.

CHAPTER 5

GPS/INS ORIENTATION ACCURACY OBTAINED VIA SIMULATION

Computer simulation studies have been performed for several reasons: to assess the orientation accuracy of inertial sensors with different error characteristic; to determine the effect of GPS aiding on attitude errors; to determine the optimal GPS update parameters for integration.

Since simulations cannot reflect actual flight conditions due to oversimplified aircraft dynamics, the results coming from these studies are taken more or less as a first approximation. The advantages of this process lie in the flexibility of testing different sensor configurations and processing methods using an errorless trajectory reference.

5.1 Simulation Flowchart

The simulation process can be divided into the following steps:

1. simulate a trajectory,
2. compute the gravity anomaly along the trajectory,

3. compute INS errorless output at a chosen data rate along the true trajectory,
4. simulate INS measurements containing sensor errors,
5. compute GPS position and velocity along the trajectory assuming an error model,
6. process INS and GPS data by different Kalman filters.

Different programs were used to accommodate computation needs in each step. The trajectory and gravity anomaly simulation used an existing program. The INS measurement computation took advantage of the DREO software package core developed by Honeywell Avionics. The GPS position and velocity simulation program has been written as part of this research and an INS/GPS processing software has been modified for the specific requirements of this project.

Since some of the inertial sensor errors are affected by vehicle dynamics, a trajectory with characteristic manoeuvres of an aircraft in a survey mission has been modelled. The trajectory consists of straight flight lines with terminal circular curves and the aircraft is accelerating from zero velocity to the operational speed of 150 m/s. The duration of the flight is 40 minutes. A motion model generated by the summation of a set of sinusoidal waves has been applied to represent irregular aircraft motion.

5.2 Specification of Measurement System Errors

The inertial sensor noise (i.e. gyro and specific force errors) has been modeled according to the Equations (2.10) and (2.11), respectively. Inertial navigation systems can be grouped in classes according to their sensors accuracies. The three systems chosen for the simulation study encompass the precise, standard and standard-low accuracy classes. Their specification parameters are listed in Table 5.1.

Table 5.1 Specification of Inertial Sensor Noise

Performance Parameters	High Precis. INS	Stand. Prec. INS	Stand-Low INS
gyro drift (deg/h)	0.001	0.01	0.2
gyro scale factor (ppm)	1	5	5
gyro misalignments (arcsec)	1	2	3
gyro random walk SD (deg/ \sqrt{h})	0.0005	0.002	0.03
gyro dither ampl.(arcsec)	150	150	150
gyro dither freq. (Hz)	512	400	400
accel. bias uncertainty (μg)	10	40	40
accel. scale factor (ppm)	50	200	100
accel. 2nd order nonlin. ($\mu\text{g}/\text{g}^2$)	10	40	40
accel. misalignments (arcsec)	2	5	7
accel. random error (μg)	1	2	2
accel. random walk SD ($\mu\text{g}/\sqrt{\text{Hz}}$)	0	0	0

Since the flight path has been chosen over an area with known gravity field, the gravity disturbance along the trajectory is computed and added to the accelerometers measurement. Thus, errors from the anomalous gravity field will affect results, because only normal gravity is assumed in the inertial mechanization (Figure 2.2).

The GPS part of the simulation takes advantage of fairly well known GPS position and velocity noise characteristics. Thus, instead of modelling GPS measurements, only the GPS filter output is simulated along the true trajectory. Table 4.2 gives the standard deviation of correlated noise and white noise for double difference GPS position and velocity. Detail classification of GPS error budget can be found in Cannon (1991) and Schwarz et al. (1993).

Table 5.2 Specification of DD GPS Position and Velocity Noise

Position Correlated Noise RMS	Position White Noise RMS	Velocity Correlated Noise RMS	Velocity White Noise RMS
0.1 m	0.005 m	0.01 m/s	0.05 m/s

According to these values the GPS position and velocity errors have been modelled by a combination of a Gauss-Markov process and white noise. The random model for GPS position errors, developed in Schwarz et al. (1993) by fitting the empirical estimated power spectral density, is given by

$$S_p(\omega) = \frac{2\beta\sigma_p^2}{\omega^2 + \beta^2} + Q_n \quad (5.1)$$

where σ_p^2 is the variance of correlated noise, β characterize correlation time length and Q_n is the spectral density of the white noise determined by the variance σ_n^2 . Since the errors in GPS derived velocity are dominated by uncorrelated noise, only a white noise model has been used for describing the GPS velocity errors.

5.3 Attitude Errors From Simulation

The inertial measurements from sensors of different accuracy (according to Table 5.1) have been generated along the same trajectory. Integration of these measurements gives inertial navigation parameters and their comparison to the modelled trajectory shows the orientation performance of stand-alone inertial navigation systems.

The statistical characteristics of attitude errors for all three systems computed for the entire mission are given in Table 5.3. Figure 5.1 depicts, in detail, errors in pitch, roll and azimuth for a medium accuracy INS during the second half of the flight mission. Pitch and roll errors are dominated by the Schuler frequency, which modulates the initial misalignment, and by constant gyro bias. The peaks reach 1.5 and 2 arc minutes and occurs at time intervals, as expected from the Schuler frequency.

Table 5.3 INS/GPS Attitude Performance From Simulation

System Accuracy Class (Gyro Drift)	GPS position & velocity aiding	Attitude Error (30 minutes)		
		pitch (STD)	roll (STD)	azimuth (STD)
precise (0.001 deg/h)	no	2"	2"	1-2"
medium (0.01 deg/h)	no	40"	50"	50"
	50 seconds	10"	15"	30"
medium-low (0.2 deg/h)	no	1'25"	1'50"	5'
	40 seconds	30'	45"	3'

In order to reduce the magnitude of the INS orientation errors the simulated information about GPS, position and velocity have been used to update the inertial mechanization. Generally, the strategy in decentralized INS/GPS integration is to update the INS filter by results from the GPS filter at every GPS epoch to obtain an optimal global estimate for position and velocity. The attitude errors for medium accuracy INS with 2 second GPS position and velocity update are shown in Figure 5.2. This type of integration dampens the Schuler type orientation errors but introduces a high frequency noise in pitch and roll estimation (see Figure 5.2). It would be, therefore, preferable either to extend the update interval or to reduce the weight of the update.

The selection of the GPS update rate for optimal attitude estimation should be based on the spectral characteristics of the two data streams. The INS position and velocity errors are mainly concentrated in the low frequency portion of the error spectra. On the other hand, the

GPS position and velocity error behaviour is mostly characterized by high frequency noise. The power spectral density of the INS and GPS velocity errors (Schwarz et al. 1993) shows that within a one minute time interval both errors become of the same magnitude. Empirically, the GPS update rate for optimal attitude estimation has been found at 50 and 40 seconds for a strapdown system of the medium and medium-low accuracy class, respectively. As displayed in Table 4.1, the attitude performance of these INS/GPS systems improved more than twice through GPS updating at these intervals. When integrating the inertial system of the highest accuracy, the gyro drift of 0.001 degree per hour is so small that it is not improved by GPS assistance within the duration of the simulation. However, the high cost of such a system (Schwarz et al. 1994) usually prevents its use in airborne remote sensing.

The simulation results have indicated that attitude accuracies of 10, 15 and 30 arc seconds in pitch, roll, azimuth are theoretically achievable by optimally aiding a medium accuracy INS with DD GPS position and velocity data. Such a performance would satisfy a vast number of airborne applications. However, not all attitude error sources listed in Equation (4.2) have been considered during the simulation. First, additional errors in attitude can be introduced by high angular velocity due to extensive aircraft dynamics. Second, the magnitude of gyro random errors may be somewhat optimistic and not correspond to those in actual flight conditions. Also, the orientation errors due to imperfect synchronization of both measurement systems have not been considered in the simulation. These uncertainties will be investigated in subsequent chapters.

Figure 5.1 INS Attitude (Gyro Drift $0.01^\circ/\text{h}$)

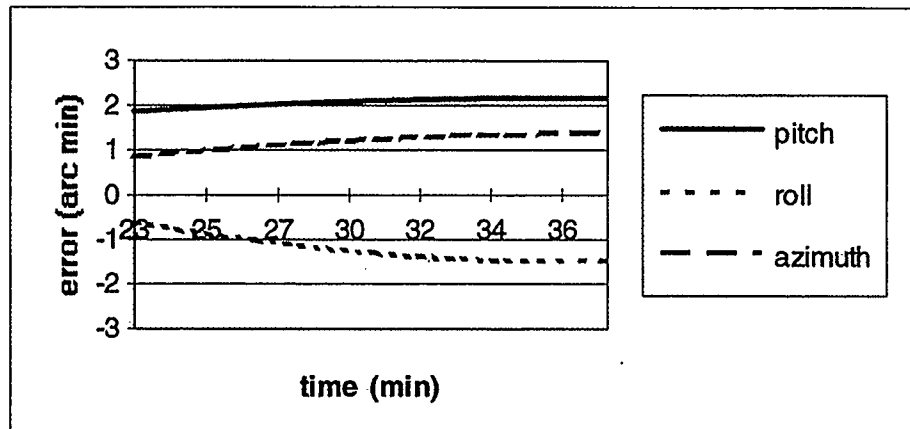


Figure 5.2 INS Attitude with 2 Sec GPS Update (G. Drift $0.01^\circ/\text{h}$)

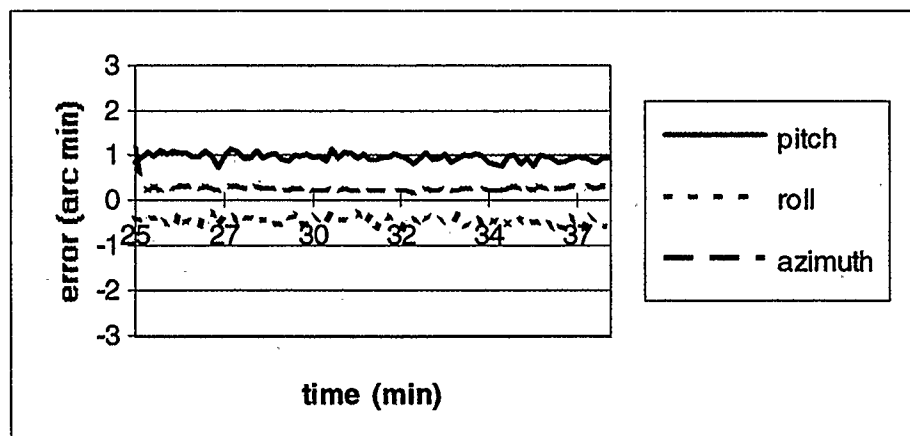
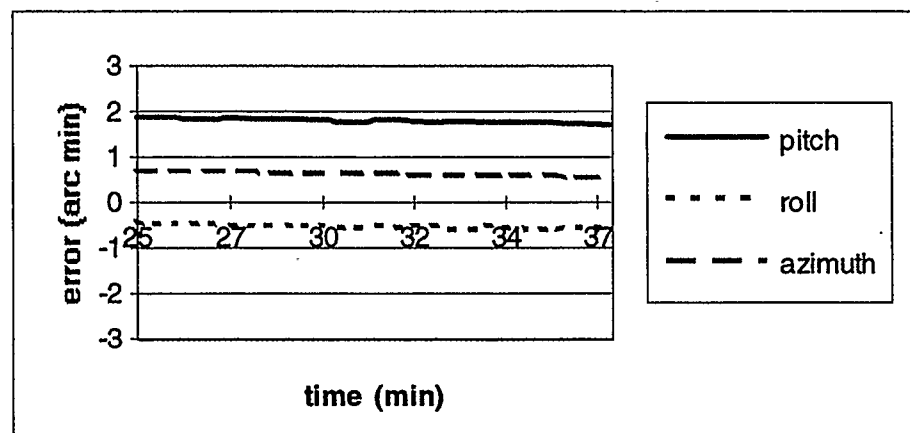


Figure 5.3 INS Attitude with 50 Sec GPS Update (G. Drift $0.01^\circ/\text{h}$)



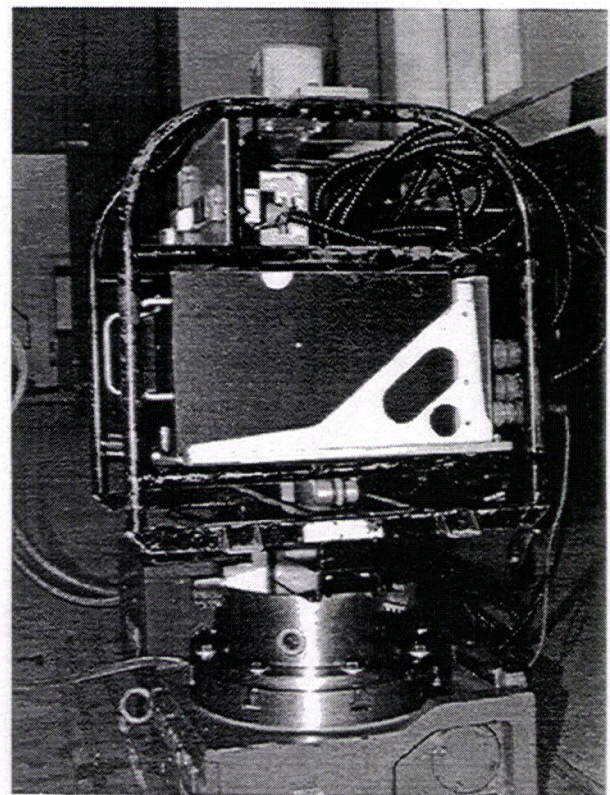
CHAPTER 6

STABILITY OF GYROSCOPES

Before assessing the INS/GPS orientation performance under actual flight conditions, gyroscope stability has been examined under high angular velocity in a lab environment. The main objective of this test was to determine whether high angular velocity due to extensive aircraft dynamic could introduce additional orientation errors, which have not been considered within the attitude error model described in Chapter 4.

The tested INS was the Ring Laser Gyro Strapdown Inertial Surveying System LTN-90-100 of the Department of Geomatics Engineering at The University of Calgary. The systems was originally designed for aircraft navigation and was modified by the

**Figure 6.1 LTN-90-100
on Rotation Platform**



manufacturer for high-resolution data output. The gyro drift of 0.02 degree per hour and the sensor's overall performance puts the LTN-90-100 into the medium accuracy group of inertial navigation system. A more detailed description of the system can be found in Wong (1988).

6.1 Test Design

The LTN-90-100 has been tested on a rotation platform provided by The U of C Mechanical Engineering Department. The computer operated platform is capable of rotations with different angular velocities up to 20 degrees per second while providing independent attitude reference with an accuracy of 3 arc seconds. As will be shown later, the rotation dynamics of a surveying aircraft rarely exceeds these angular rates. Since the rotation platform has only one degree of freedom in the horizontal plane, only the vertical gyro can be exposed to the rotation. However, the repeatability of pitch and roll determination at different azimuths can also be evaluated. The test set-up is displayed in Figure 6.1, which shows the LTN-90-100 mounted in a frame and connected to the axis of the rotation platform.

After 20 minutes of static alignment a pattern of rotation sequences has been repeated within a time period of 45 minutes. As shown in Table 6.1 each sequence contains 14 rotations with angles of different magnitude and sign. Since the time between each rotation is set to be 20 seconds one rotation sequence is completed within 7 minutes. The angular velocity was set at 5 and 10 degrees per second during the first two rotation sequences and kept at 20 degrees per second for the next five series.

Table 6.1 Rotation Sequence

Rotation (°)	10	-10	20	-20	45	-45	90	-90	180	-180	720	-720	-1440	720
--------------	----	-----	----	-----	----	-----	----	-----	-----	------	-----	------	-------	-----

6.2 Data Analysis And Results

Since the rotation platform provides a better reference for IMU angles than for angular velocities, the system's capability of determining relative angles is tested.

The initial azimuths acquired after the alignment procedure and orientation of the rotation table was considered as a reference for the IMU derived angles. The relative azimuth errors for all rotations are depicted in Figure 6.2. Each rotation seems to have an error of 20 arc seconds. This is most likely due to the quantization effect. In other words, the rotation platforms suddenly accelerates from zero to 20 degree/sec. This acceleration has an impulse behaviour which, due to limited sensor resolution, causes a 'jerk' in the attitude output. According to the LTN-90-100 technical manual, a limited bit output sets the vertical gyro resolution to 0.003906 degree/sec or in terms of angular magnitude to 19.8 arc seconds. However, such rapid acceleration can be hardly expected under aircraft dynamics. The errors in relative angle determination after removing the quantization effect (Figure 6.3) are within 15 arc seconds during the first two rotation series. The repeatability of determining these angles is 30 arc seconds after 45 minutes. Since a similar error behaviour can be found for angles of different magnitude, the influence of high angular rate is questionable. They are

mainly caused by gyro random noise, dither and quantization error. Their time growing trend is caused by gyro drift. Much the same behaviour can be detected for the roll determination (Figure 6.4). Since the LTN-90-100 was aligned in the east direction, the roll determination is more accurate at 90° , because sensor biases have been estimated in this direction.

The results of testing the LTN-90-100 vertical gyroscope under different angular velocities indicate that a high angular rate of up to 20 degree/sec did not introduce additional constant errors for the attitude determination within the control platform resolution. In other words, the system is capable of following the orientation dynamics of a surveying aircraft.

Figure 6.2 LTN-90-100 Relative Azimuth Determination, $\omega = 20$ deg/s

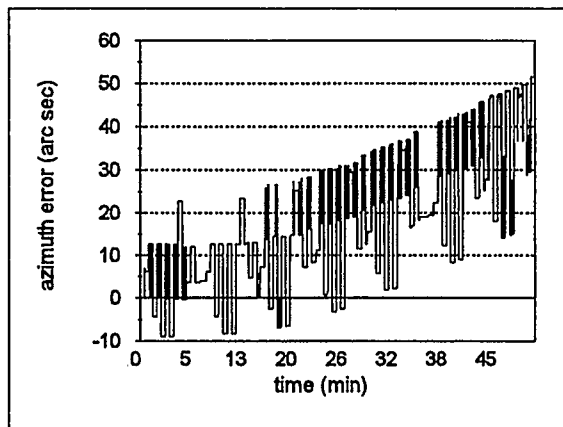


Figure 6.3 Relative Azimuth Determination Without Quantizer Effect

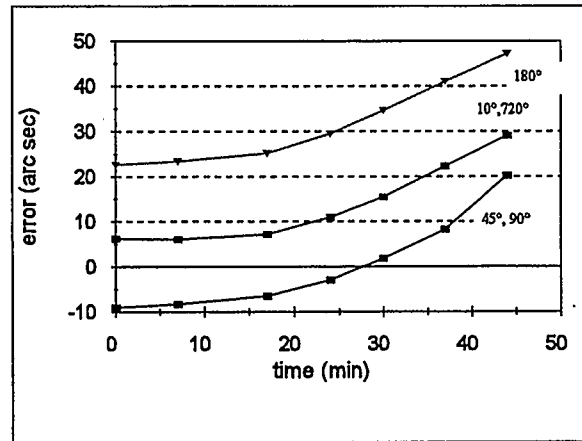
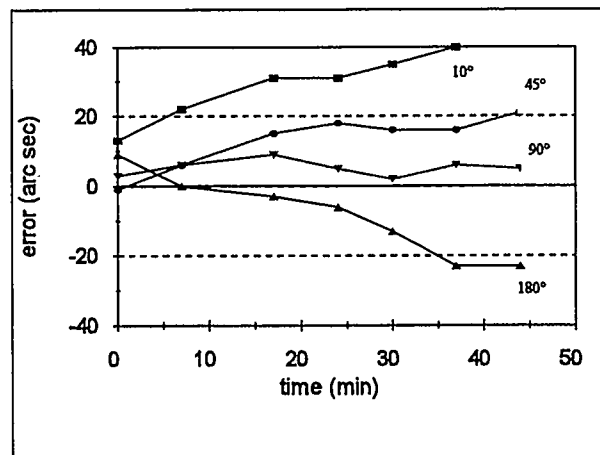


Figure 6.4 Repeatability of Roll Determination at Different Azimuths

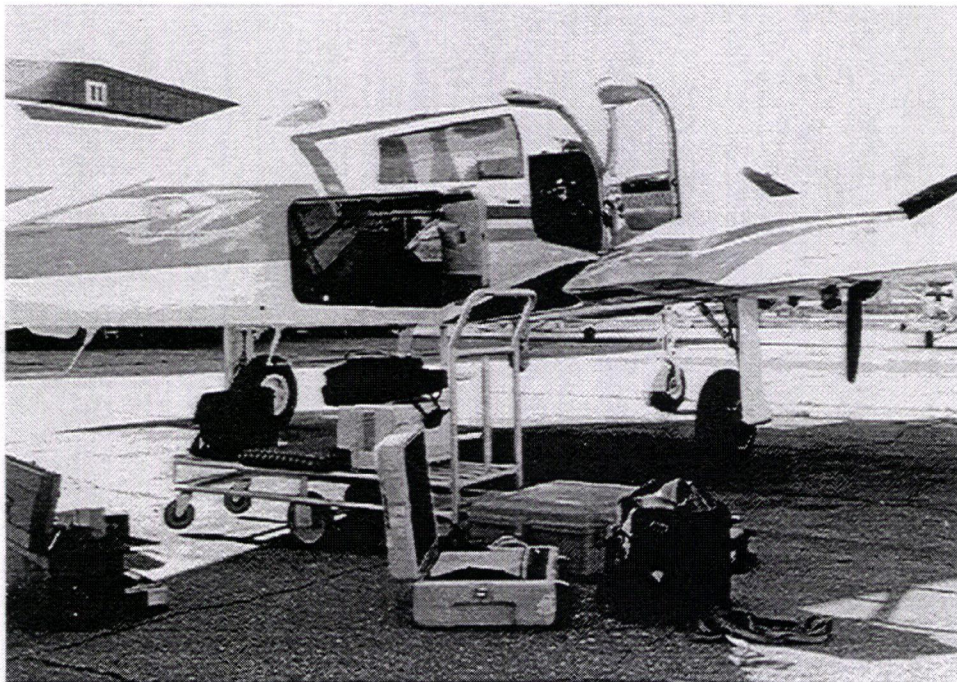


CHAPTER 7

INS-GPS-PHOTOGRAMMETRY AIRBORNE TEST

An airborne test has been designed to support simulation results and clarify remaining uncertainties in INS/GPS orientation accuracy, i.e. the magnitude of gyro noise under flight conditions and the orientation errors due to the imperfect synchronization of measurement systems.

Figure 7.1 Equipment Being Loaded into the Airplane



To assess the in-flight orientation accuracy of an INS/GPS system, an independent data stream of superior accuracy is needed. The principle of inverse photogrammetry is used here to provide a basis for attitude comparison. A medium scale photogrammetric test with INS/GPS sensors on board is described and the photogrammetric data are used to evaluate the camera attitude accuracy. The INS/GPS orientation performance is then investigated using the camera attitude as a reference. Afterwards, predicted accuracies from simulations are compared with actual test results and the differences are explained by analyzing the INS signal in the frequency domain.

7.1 Attitude Derived from Inverse Photogrammetry

By mounting a camera on a rigid platform together with the INS, a precise orientation angle difference between the INS and the camera can be derived. The processing method used to derive the camera orientation is a photogrammetric bundle adjustment.

The bundle adjustment takes advantage of the geometric strength of overlapping photographic images. Each image is comprised of a bundle of imaging rays which forms a strong connection between the object space (terrestrial coordinate frame) and the exposure stations along the flight path. As such, the flight path is represented by a sequence of perspective centres corresponding to the time of camera exposure. At that time, position and orientation of camera perspective centres (parameters of exterior orientation) are precisely defined by the geometry of the photogrammetric bundles.

The parameters of exterior orientation can be derived via the relationship between the object space and the image space. This connection is usually formulated by means of collinearity equations. The collinearity equations express the condition that the perspective centre, an object space point and its corresponding image all lie on a straight line. This can be mathematically formulated as

$$\begin{aligned} x_p &= -f \left[\frac{m_{11}(X_p - X_0) + m_{12}(Y_p - Y_0) + m_{13}(Z_p - Z_0)}{m_{31}(X_p - X_0) + m_{32}(Y_p - Y_0) + m_{33}(Z_p - Z_0)} \right] \\ y_p &= -f \left[\frac{m_{21}(X_p - X_0) + m_{22}(Y_p - Y_0) + m_{23}(Z_p - Z_0)}{m_{31}(X_p - X_0) + m_{32}(Y_p - Y_0) + m_{33}(Z_p - Z_0)} \right] \end{aligned} \quad (7.1)$$

where, X_p, Y_p, Z_p and x_p, y_p are the point coordinates in the geodetic reference system and in the image coordinate system, respectively; X_0, Y_0, Z_0 are the coordinates of camera perspective centre in the geodetic reference system; f is the camera focal length and the subscripted m symbolizes the rotation matrix coefficients. Three angles (ω, ϕ, κ) inherent in this matrix represent rotations around coordinate system axes.

Collinearity equations in the linearized form (see Wolf 1983) can be written for each control point. Each such equation contains six unknowns ($X_0, Y_0, Z_0, \omega, \phi, \kappa$) per unique exposure and when dealing with individual images at least three control points are needed to find these parameters. However, connections between multiple images can be formed by measuring points common to adjacent images and by enforcing intersection constraints between them.

In such cases, a strip or block of images can be constructed with only a minimal amount of ground control information. On the other hand, redundant control points help reduce the error propagation within the strip or bundle adjustment and this improves the accuracy of derived parameters of exterior orientation. Nevertheless, the resulting camera attitude and position are strongly correlated. This correlation can be decoupled by introducing GPS observations for camera perspective centre positions into the bundle adjustment (Kenefick 1972). Equation (7.1) can be modified for GPS input as

$$\begin{pmatrix} X_p \\ Y_p \\ Z_p \end{pmatrix} = \begin{pmatrix} X \\ Y \\ Z \end{pmatrix}_{\text{GPS}} + \mathbf{M}_m^c \begin{pmatrix} X \\ Y \\ Z \end{pmatrix}_{\text{offset}} + \alpha (\mathbf{M}_m^c)^T \begin{pmatrix} x_p \\ y_p \\ -f \end{pmatrix} \quad (7.2)$$

where $(X, Y, Z)_{\text{GPS}}$ represent GPS antenna position at the time of camera exposure; $(X, Y, Z)_{\text{offset}}$ is the displacement between the GPS antenna and the camera perspective centre; α is a point dependent scale factor and \mathbf{M}_m^c symbolizes the rotation from the mapping plane to the photo plane given as

$$\mathbf{M}_m^c = \mathbf{R}_x(\omega) \cdot \mathbf{R}_y(\phi) \cdot \mathbf{R}_z(\kappa) = \begin{pmatrix} \cos \phi \cos \kappa & \cos \phi \sin \kappa & -\sin \phi \\ \sin \omega \sin \phi \cos \kappa - \cos \omega \sin \kappa & \sin \omega \sin \phi \sin \kappa + \cos \omega \cos \kappa & \sin \omega \cos \phi \\ \cos \omega \sin \phi \cos \kappa + \sin \omega \sin \kappa & \cos \omega \sin \phi \sin \kappa - \sin \omega \cos \kappa & \cos \omega \cos \phi \end{pmatrix} \quad (7.3)$$

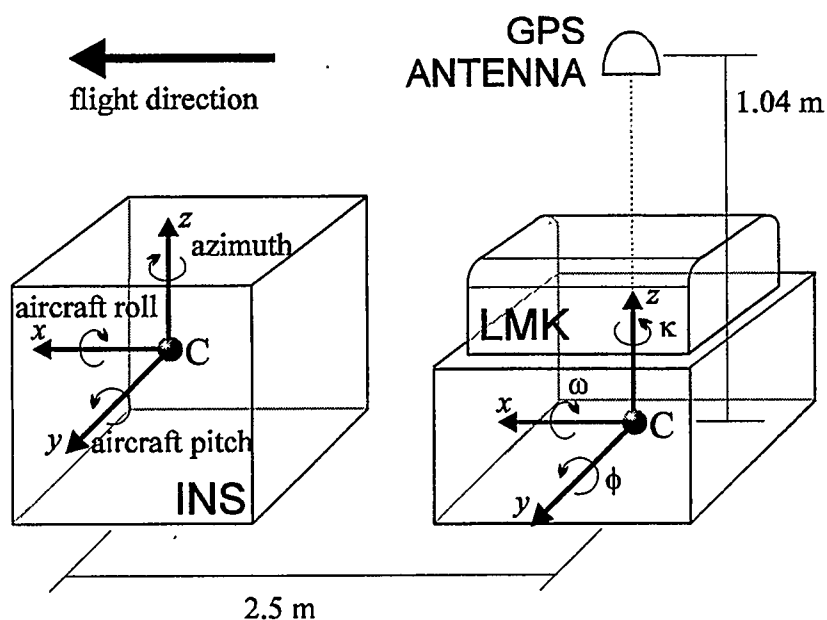
The order in which three rotations ω , ϕ , κ are applied affect the error propagation in the rotation matrix (Blais 1979). This appears to be minimized when using order ω , ϕ , κ in \mathbf{M}_c^m (i.e. starting the rotation with small angles). Before attitude comparison between the INS and the aerial camera can be made, both orientation parameters have to be referred to the same coordinate system. Since the INS attitude matrix expresses the rotation between INS body frame and the local-level frame (Chapter 2, Section 2.4), \mathbf{M}_m^c has also to be related to the system of geodetic coordinates. The photogrammetric model is flexible with regard to the choice of a datum, but it has to be projected into the plane. Therefore, the chosen map projection has to represent a system of curvilinear geographic coordinates and also be conformal in order to perform angle comparisons. Both these requirements can be satisfied when using the Transverse Mercator (TM) projection. In the TM projection, the reference ellipsoid is conformally projected onto a cylinder contacting with the ellipsoid along the central meridian. The position of the central meridian can be chosen in the middle of the flight area in order to minimize the azimuth correction due to meridian convergence. Since the rotation around the z-axis has been chosen as primary in Equation(7.3), the meridian convergence can be directly added to κ . This correction changes \mathbf{M}_m^c to \mathbf{M}_l^c . Both INS and camera attitude are now referenced to the local level frame and thus can be compared.

7.2 INS-Camera Offset Determination

Following Skaloud et al (1994), a key assumption for attitude comparison is that no changes in relative position and orientation between the camera, INS and GPS antenna occur. This can

be achieved by hard mounting the GPS antenna and INS to a rigid platform on the aircraft and by locking the camera down to the same platform. Even if there is only a small separation between the different sensors, it must be compensated for by introducing a GPS-camera translation vector and a GPS-INS vector to the bundle adjustment (Equation 7.2, Figure 7.2). A camera-INS differential rotation also has to be determined for attitude comparison or for image georeferencing in real applications.

Figure 7.2 INS-GPS-Camera Offset Determination



Since the centre of the INS as well as the perspective centre of the camera is marked on the outside of both devices, their translation vectors can be measured by using conventional surveying methods. Determination of the camera-INS differential rotation matrix (ΔR_b^c) is more complicated, because the sensor axes in both devices cannot be physically observed and

will have to be computed indirectly via in-flight calibration. The condition equation used for the $\Delta \mathbf{R}_b^c$ computation is:

$$\mathbf{M}_1^c = \Delta \mathbf{R}_b^c \cdot \mathbf{R}_1^b \quad (7.4)$$

where, \mathbf{R}_1^b is part of the INS output and denotes the rotation matrix between the local-level frame and the INS body frame. When using the TM projection as a mapping plane, \mathbf{M}_1^c as well as \mathbf{R}_1^b refer to the local-level frame. Consequently, $\Delta \mathbf{R}$ can be computed from Equation (7.4) by multiplying \mathbf{M}_1^c by the transposed \mathbf{R}_1^b (orthogonal matrix property, i.e. transposition equals the inversion). Three rotation angles $\Delta \varphi$, $\Delta \theta$, and $\Delta \alpha$ can be extracted from $\Delta \mathbf{R}_b^c$ using the formulas shown in Equation (7.5) which use the rotation matrix structure shown in Equation (7.3)

$$\begin{aligned} \Delta \theta &= \tan^{-1} \left(\frac{\mathbf{R}_{23}}{\mathbf{R}_{33}} \right) \\ \Delta \varphi &= \sin^{-1}(-\mathbf{R}_{13}) \\ \Delta \alpha &= \tan^{-1} \left(\frac{\mathbf{R}_{12}}{\mathbf{R}_{11}} \right) \end{aligned} \quad (7.5)$$

Since the bundle adjustment yields one \mathbf{M}_1^c for each camera exposure and the INS output can be interpolated for these events, differential rotation angles can be computed for each

photograph acquired during the flight mission. Moreover, their variations indicate the actual INS/GPS orientation performance assuming the camera orientation errors to be insignificant.

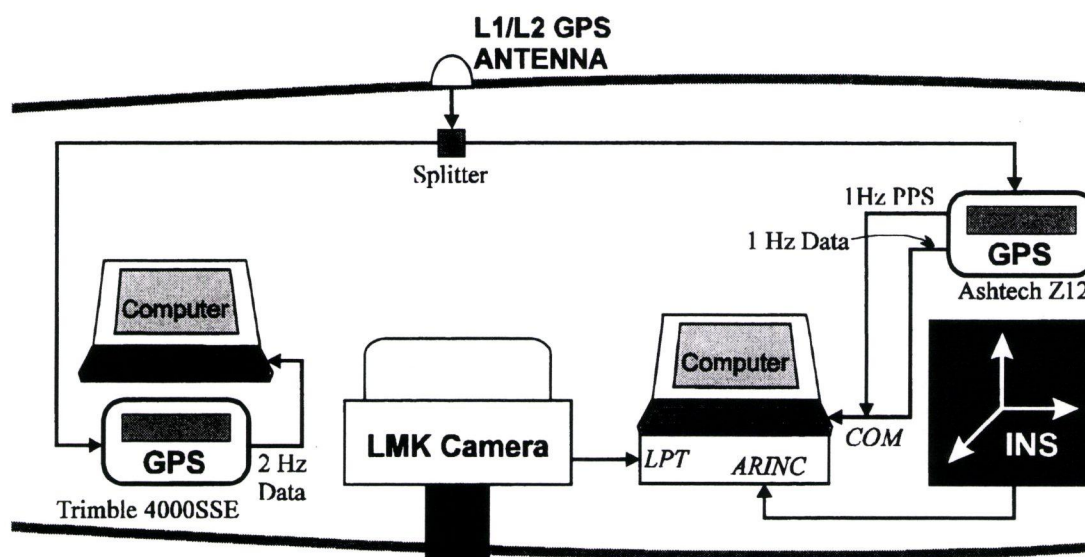
7.3 Equipment Selection and Test Design

The geodetic receivers selected for the test are pairs of high performance C/A code Trimble 4000 SSE and P-codeless Ashtech Z12. Both types of receivers are dual frequency receivers and are equipped with L1/L2 antennas. Each pair creates an independent base station-rover pair for relative positioning. The photogrammetric camera installed in the aircraft is a Zeiss LMK aerial camera with a precise shutter pulse output. The inertial navigation system to be tested is a Litton LTN-90-100 strapdown system with gyro drift rate of about 0.02 deg/hour.

The actual aircraft installation is depicted in Figure 7.3. The GPS signal coming from the aircraft's L1/L2 is split between the Ashtech and the Trimble GPS receivers. The Trimble 4000 SSE generates full positional and measurement data twice per second which are stored in a notebook computer. The other data collection system receives 64 Hz raw inertial data via a high speed ARINC interface together with the 1 Hz Ashtech GPS data. The Ashtech also provides a precise 1 pulse per second (PPS) output which is recorded together with the computer time. A camera pulse is generated during the illumination of the fiducials for each camera exposure. The camera pulse and INS data are stamped by the internal computer clock so that a common time frame is established. The GPS antenna is mounted on the aircraft fuselage directly above the camera centre. The INS unit is placed beside the aerial camera and

both devices are locked down to the same platform so that their orientation with respect to each other is fixed.

Figure 7.3 Aircraft Installation



The configuration of ground control has been designed to derive the camera orientation with the highest accuracy. Altogether, 17 control points have been evenly distributed on both sides of each flight line supplying strong geometry for attitude determination. Their 3-D coordinates were determined by adjusting a network of 25 GPS static baselines. The relative positioning accuracy of the network points was 2 parts per million. Three flight lines were flown over the city of Calgary in early July 1994. Each flight line was about 10 km long and contained 12-14 photographs. Together, they form the photogrammetric block with 60% forward and 20% side overlap. At an average flying height of 1500 m and with a 15 cm camera focal length the photo scale was 1:10 000.

The GPS base station receiver (Trimble 4000 SSE) was placed on the network origin located in the middle of the block. The coordinates of the camera projective centres were interpolated from positions computed from differential carrier phase measurements using two Trimble 4000 SSE receivers operating at 2 Hz. Since the Ashtech data were collected at one second intervals this solution was not suitable for precise interpolation and was only used as auxiliary control. Due to a GPS signal discontinuity during the aircraft turns the ambiguity was determined on-the-fly in the second and third flight lines.

7.4 Photogrammetric Results

The measurements were adjusted as a block using a bundle method implemented in the GPSBUND software (Cosandier 1994). Positions of the camera perspective centres, obtained from the GPS solution, were heavily weighed ($\sigma = 0.05$ m), in order to minimize the correlation between unknown position and orientation parameters. For the same reason, drift parameters were not introduced in the adjustment. However, self-calibration for a focal length adjustment was performed. For precise attitude determination, the bundle adjustment was run using all control points. In order to check the predicted orientation accuracy, flight lines 1, 2 and 3 were adjusted with only 11 control points and the remaining 6 control points were included as check points for error estimation.

Adjustment results are shown in Table 7.1. RMS values of check point residuals are less than 10 cm and indicate a very good solution for a medium scale photogrammetric block. Photo

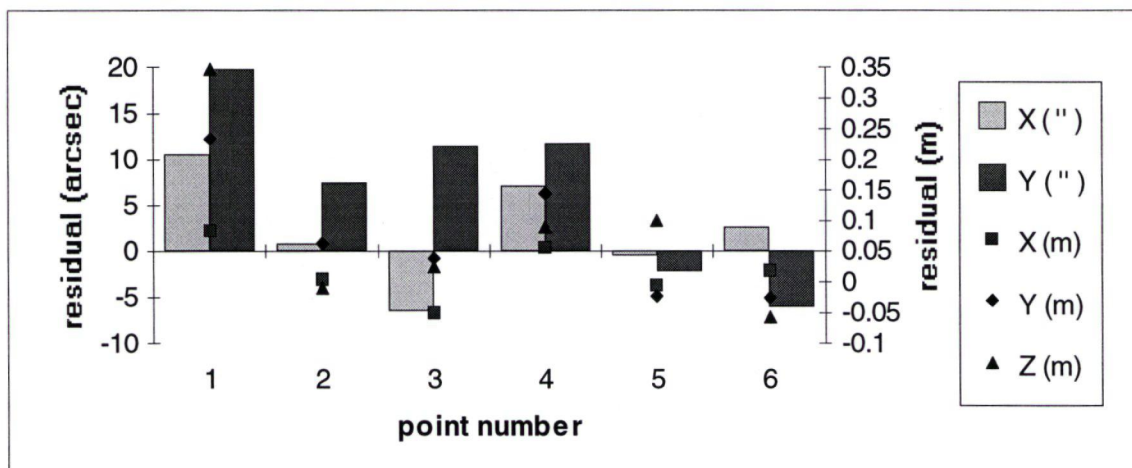
residuals are also in good agreement with control point residuals reaching the limit of camera resolution and targeting precision.

Table 7.1 Bundle Adjustment Results

	X	Y	Z	no.
Airborne GPS RMS (m)	0.07	0.10	0.05	39
Photo residuals RMS (mm)	0.0055	0.0052	-	1587
Control points RMS (m)	0.04	0.05	0.03	11
Check points RMS (m)	0.04	0.08	0.07	6
Check points RMS (arcsecond)	6	12	-	6

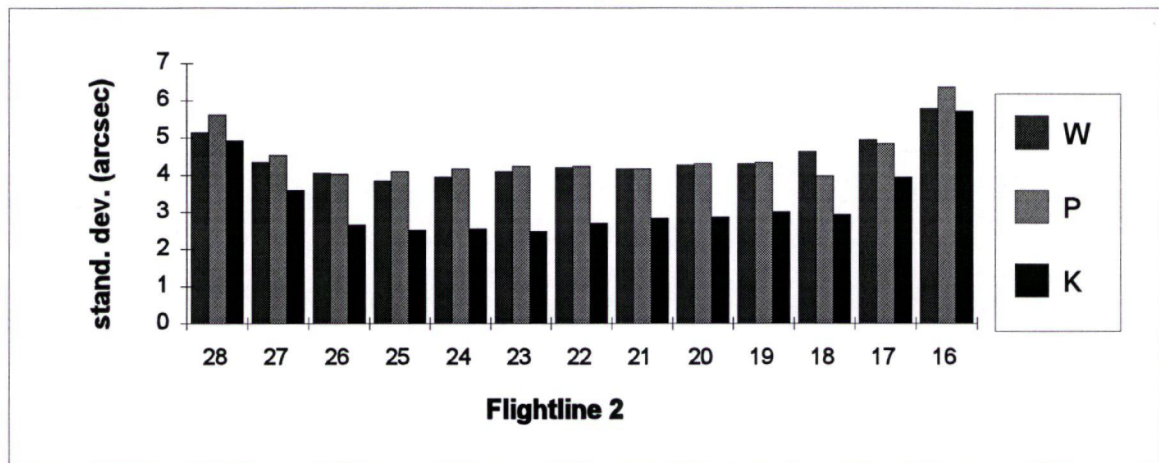
The check point residuals depicted in Figure 7.4 can be considered as an independent verification of the photogrammetric results. Moreover, being converted to equivalent angular quantities they also indicate the maximum errors caused by camera misorientation.

Figure 7.4 Check Point Residuals



Due to the geometric configuration, the predicted attitude accuracy is generally better for photographs within the strips than those towards the end (Figure 7.5). The theoretical accuracy of the attitude angles derived from bundle adjustment is in the range of 3-6 arc seconds. Thus, the camera orientation parameters are determined with an accuracy which is two to four times better than that expected from the tested INS.

Figure 7.5 Predicted Camera Orientation Accuracy



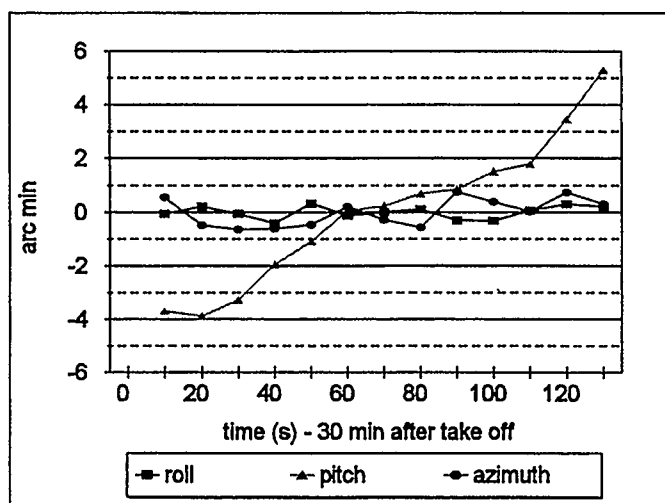
7.5 INS/GPS Orientation Performance Analysis

A GPS/INS integration software KINGSPAD (KINematic Geodetic System for Positions and Attitude Determination) developed at The University of Calgary, has been modified to process data according to the methodology discussed in Chapter 4. KINGSPAD employs a 15 state decentralized Kalman filter (Figure 4.1) and is able to process INS and GPS data separately or in the form of integration. In the integration mode, the program delivers up to

64 Hz navigation output, which allows to precisely interpolate attitude for the time of camera exposure. The program written as a part of this research will use GPSBUNDL and KINGSPAD output to perform such interpolation and compute variations in INS-camera attitude by utilizing formulas (7.3)-(7.5).

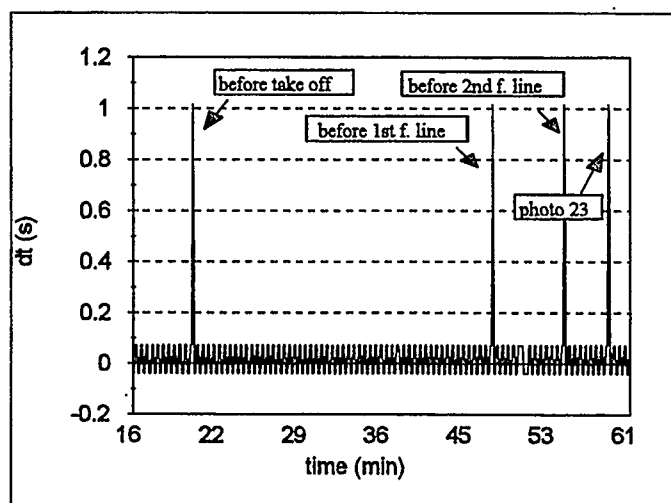
Processing the INS data in free navigation mode (without GPS updates) indicated a large data gap during the turn between the second and third flight lines which destabilized the entire solution from this point on. Therefore, only results from the first two flight lines are evaluated. Moreover, since a few missing epochs have been found towards the end of the second flight line, this period also has not been considered. The variations in INS-camera relative orientation after removing the mean values in the first two flight lines are 13 arcseconds in roll and 30 arcseconds in azimuth. They are depicted in Figure 7.6 and show random behaviour. However, the error in pitch indicates a systematic drift of 3 arc minutes per minute.

Figure 7.6 Variations in INS-Camera Orientation



Since the overall pitch and roll accuracy should be similar, there is no obvious reason for such a drift. A possible explanation would be a system misalignment of several degrees. In that case, the amplitude of the Schuler loop would be so large that it would significantly affect the short-term attitude determination. However, since the GPS position and velocity aiding tends to dampen attitude errors due to the initial misalignment over time (Chapter 4), the large misalignment would have had to occur during the flight before the first flight line. This is highly unlikely! An analysis of the raw inertial data indicated problems in data continuity caused by the logging hardware (Figure 7.7). Although the 0.1 second time jump depicted in Figure 7.7 reflects only problems in computer clock reading, the 1 second time intervals indicates data is missing. While the first data gap occurred during the alignment procedure and, therefore, does not have to be considered, the second took place during the aircraft turn before entering the first flight line. At that time, the aircraft was already heading north but the roll was still subject to the dynamics of several degrees per second, which leads to a misalignment mainly in the east direction.

Figure 7.7 INS Data Discontinuity



The effect of small misalignment errors on the attitude matrix can be written as

$$\tilde{\mathbf{R}}_b^1 = \begin{pmatrix} 1 & -\varepsilon_z^1 & \varepsilon_y^1 \\ \varepsilon_z^1 & 1 & -\varepsilon_x^1 \\ -\varepsilon_y^1 & \varepsilon_x^1 & 1 \end{pmatrix} \mathbf{R}_b^1 \quad (7.6)$$

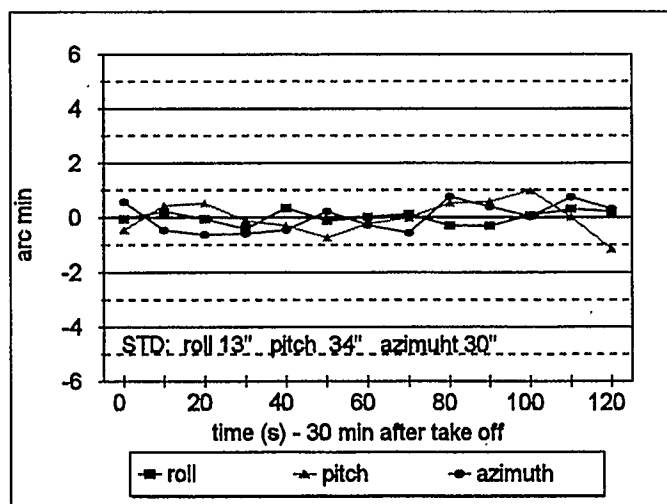
where the INS attitude matrix \mathbf{R}_b^1 is given by definition. Errors in pitch (θ), roll (φ) and yaw (ψ) due to the misalignment can be found by extracting these angles from Equation (7.6) as

$$\begin{aligned} \delta \theta &= \varepsilon_e^1 \cos \psi + \varepsilon_n^1 \sin \psi \\ \delta \varphi &= -\varepsilon_e^1 \frac{\sin \psi}{\cos \theta} + \varepsilon_n^1 \frac{\cos \psi}{\cos \theta} \\ \delta \psi &= \varepsilon_e^1 \sin \psi \tan \theta - \varepsilon_n^1 \cos \psi \tan \theta + \varepsilon_z^1 \end{aligned} \quad (7.7)$$

Obviously, Equation (7.7) yields large errors only in pitch when the misalignment is mostly in east direction and the yaw is close to zero, as it would be in this case. Moreover, the attitude error due to the system misalignment becomes immediately modulated by the Schuler frequency. The error in pitch is drifting by 3'/minute which would correspond to a Schuler oscillation with an amplitude of several degrees, generated by an ε_e^1 of similar magnitude. During a time period of 2 minutes the slope of the Schuler oscillation can be well closely approximated by a straight line. A correlation analysis shows that, even though the correlation coefficient for roll and azimuth is well below 0.2, the coefficient for the pitch error is 0.98. This strong correlation reflects a systematic drift in pitch most likely being caused by a

misalignment in the east direction due to the logging hardware. If this assumption is correct, the systematic part of the pitch error can be corrected by the parameters found in the correlation analysis. The variation in INS-Camera attitude with corrected pitch values are plotted in Figure 7.8. Hence, all three rotation angles now express a similar behaviour, although with an attitude standard deviation of 15 to 25 arc seconds. The variation is higher than suggested from the simulation and this disagreement will be further discussed in Section 7.7.

Figure 7.8 Variations in INS-Camera Orientation With Corrected Pitch

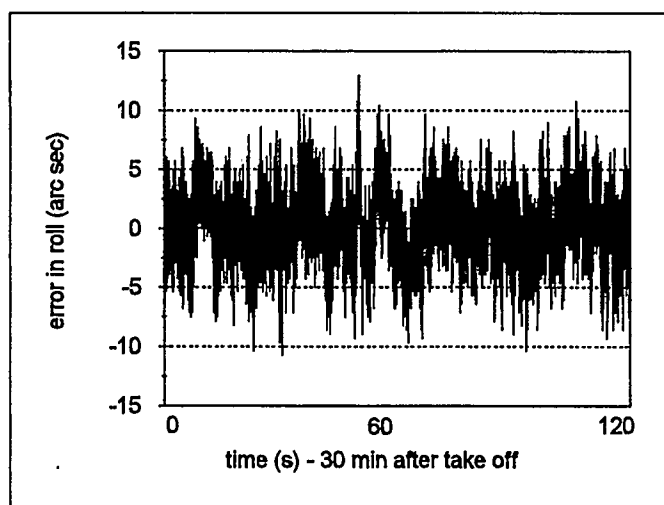


7.6 INS/GPS Measurement Delays

The attitude error model for INS/GPS integration introduced in Chapter 4 considers both data streams as perfectly synchronized. In reality, this is not true. INS measurements are passing

through a digital filter introducing an internal time delay. The magnitude of the delay depends on the filter characteristics and aircraft dynamics, which could be different for every channel. Generally, such a delay should not exceed the time span between measurement epochs (e.g. 16 ms for the LTN-90-100). The internal time delay of a GPS receiver is difficult to trace, since it is not specified by the manufacture. Other limits in the data stream synchronization are in the data logging hardware, namely in the data registration by the INS data acquisition board and in computer clock errors. To show the synchronization effect within the dynamics of the first flight line, a 5 ms delay has been introduced to the INS data stream. The error in roll determination due to such an effect is displayed in Figure 7.9.

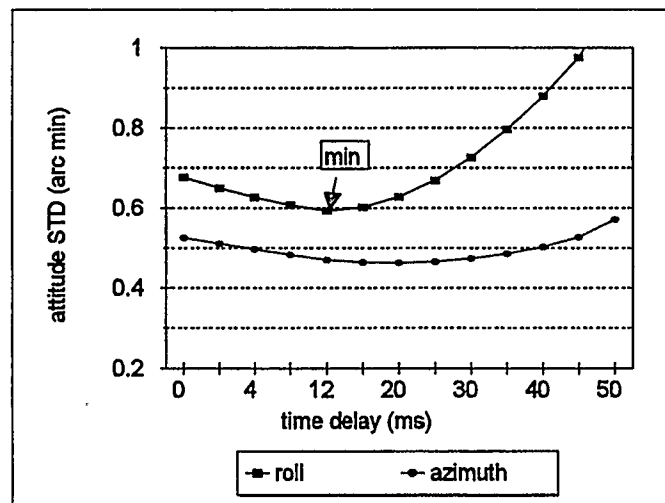
Figure 7.9 Roll Error in First Flight Line Due to a 5 ms Time Delay



These errors generally show a random behaviour with RMS values at the level of 5 arc seconds and peak values around 10 arc seconds. Practically, the INS/GPS measurement delay is very difficult to evaluate, because a trajectory reference of superior accuracy is missing.

However, using the photogrammetry derived attitude these values can be estimated at the camera exposure stations. The camera synchronization is realized by stamping a pulse generated by the illumination of the fiducials. Such a process introduces a timing error well below the 0.1 ms level and, therefore, can be taken as a reliable reference. Thus, having the camera orientation, the INS synchronization errors can be estimated by finding the minimal attitude variance between both data streams computed for different time delays. This method has been applied to the synchronized measurements in both flight lines and the results are shown in Figure 7.10. The INS synchronization errors can be most easily detected by using roll data, which has higher orientation dynamics. In both cases, the INS measurement delay is about 15 ms.

Figure 7.10 INS Time Delay Estimation



7.7 Frequency Analysis of Inertial Data

The simulation results have indicated that within a time period of two minutes the INS derived attitude should be at the level of 5 arcseconds. Considering that camera orientation can also be obtained with 5 arcseconds accuracy, the INS-camera variation obtained from the flight is about two to three times worse. Moreover, the INS simulation with optimal GPS updates produces a rather smooth behaviour of the INS attitude values requiring updates only every 40-50 seconds. However, this was in the absence of platform vibrations. To estimate the effect of the increased noise level due to aircraft vibration, raw inertial signals from different vibration environments have been analyzed in the frequency domain.

The lab test indicated that the noise level of the LTN-90-100, free of environmental disturbances, is about 3 arc second. It is mainly caused by dither effects. To observe the data in the spectral domain, the Fast Fourier Transform (FFT) is used to compute the amplitude spectra. The number of FFT points is 8192 which corresponds to a 128 second long data set. Since the dither frequency is applied at approximately 400 Hz and the acquisition board collects the data at a 64 Hz sampling rate this causes an aliasing effect in the range limited by the Nyquist frequency of 32 Hz. Figure 7.11 shows the FFT amplitude spectra of the x-gyro and x-accelerometer output in static mode. The peaks of 30, 19 and 9 Hz correspond to the 3 aliased dither frequencies.

Figure 7.11 x-Gyro and Accelerometer FFT, Lab Environment

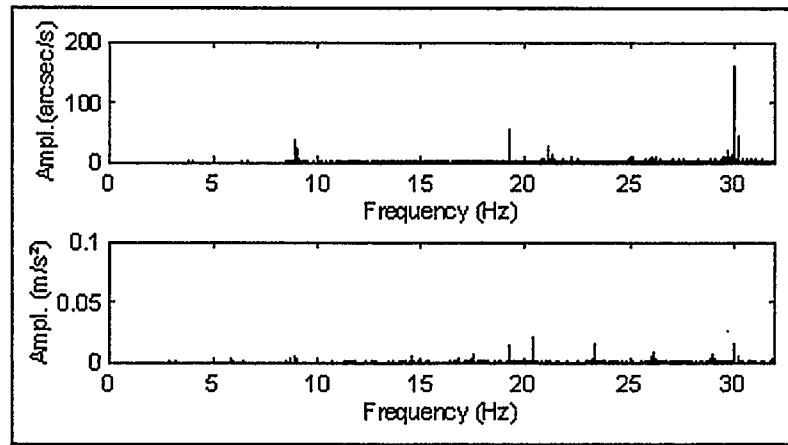
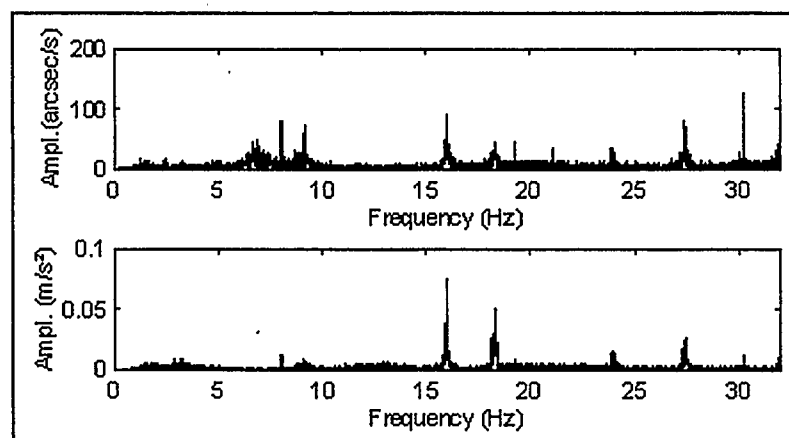


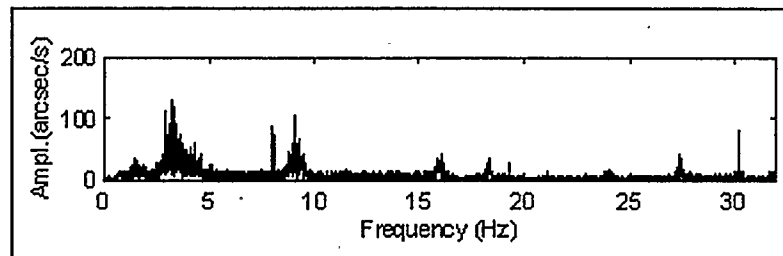
Figure 7.12 shows the x-gyro and the accelerometer spectrum with the aircraft standing on the runway, but with engines running. Several distinct spectral peaks can be identified. The aircraft movement caused mainly by differential speed of the left and the right propellers can be seen in the frequency range 5 - 7 Hz. The increased noise level due to engine vibration can be seen throughout the spectra with a significant frequency at 16 Hz, which is the frequency of propellers idling at 1000 RPM. The dither aliased frequencies are approximately at 9, 19, and 30 Hz.

Figure 7.12 x-Gyro and Accel. FFT, Aircraft Standing and Engines Running

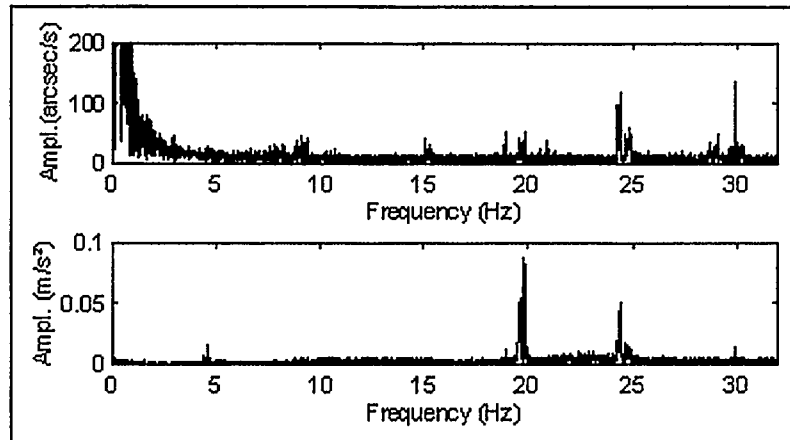


The aircraft wheel location allows more vibration along its pitch axes, which can be seen in the frequency range 1-5 Hz as depicted in Figure 7.13.

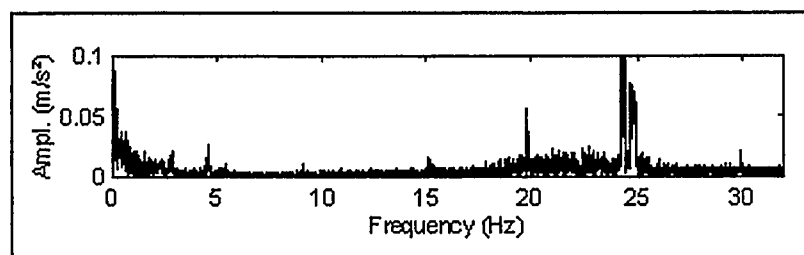
Figure 7.13 y-Gyro FFT, Aircraft Standing and Engines Running



Vibration characteristics change substantially under flight conditions. The FFT of the x- gyro and accelerometer output during the first flight line are displayed in Figure 7.14. Assuming the dynamic threshold to be 10 Hz, the engine noise is higher and more evenly distributed throughout the spectrum than in the static case. When at cruising speed, the propellers run at about 2400 RPM or, in other words, with a frequency of 40 Hz. Since such a frequency is above the Nyquist frequency, it appears aliased at 20 Hz. Hence, a large peak at this frequency in the accelerometer data corresponds to the speed of propellers. The dither effect can be mainly seen at frequencies 19, 24 and 30 Hz.

Figure 7.14 x-Gyro and Accelerometer FFT During the First Flight Line

Even though the y, z-gyro and y-accelerometer spectra are similar to those displayed in Figure 7.14, the one computed for the z-accelerometer is quite different (Figure 7.15). The vibration generated by propellers running at 40 Hz have a higher amplitude in the flight direction and substantially increase the noise level in the range of 20 - 25 Hz. Also, since operated manually, the propellers are not running with the same speed, which generates vibrations mainly along the z-axis.

Figure 7.15 z-Accelerometer FFT During the First Flight Line

A reliable estimate of measurement noise on attitude determination can be obtained by eliminating the mean value and integrating only the power in the frequencies above the aircraft dynamics. Assuming the dynamic threshold to be 10 Hz, the measurement noise has been extracted from the gyro signal by applying a high pass filter. The integrated gyro data after high pass filtering are plotted as orientation errors in Figures 7.16 and 7.17 for static and on the fly signal. In both cases, the effect of vibration on short term attitude accuracy is at the level of 10 arc seconds, about the same magnitude as the effect of a 5 ms measurement delay. Moreover, these errors seem to be randomly distributed. Overall, the magnitude and characteristic of the orientation errors due to the platform vibration explains the difference between the 'smooth' and more accurate simulated results and those obtained from actual flight test.

Figure 7.16 Error in Roll Due to Aircraft Vibration on the Runway

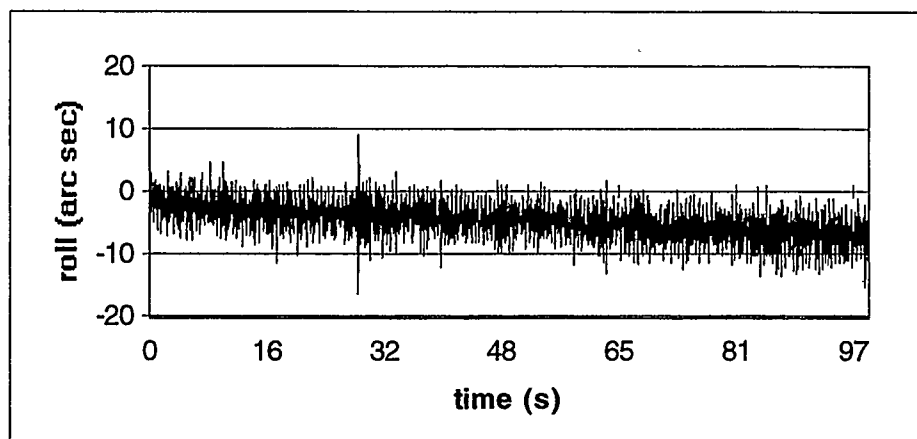
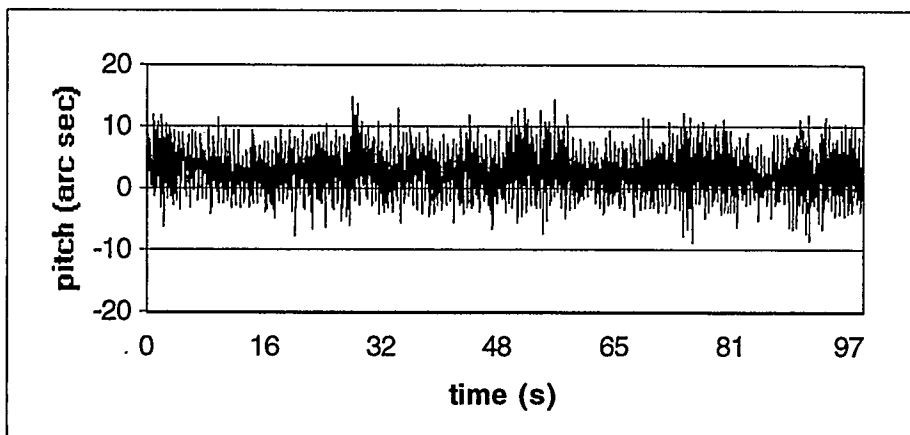


Figure 7.17 Error in Pitch Due to in-Flight Aircraft Vibrations

Theoretically, it would be possible to use a low pass filter to remove all the disturbing signals above 10 Hz, in order to improve the attitude determination. However, the Butterworth filter and other similar digital filters do not remove the frequencies above the cutoff threshold correctly. They change the mean of the data set and introduce amplitude distortion below the cutoff frequency, which could result in a deterioration of attitude accuracy. Therefore, it would be preferable to use a special filtering method for removing distinctive frequencies (e.g. dither spike removal Czompo, 1990). Such a method would remove only the dither or other easily detectable frequencies from the spectrum while leaving the mean unchanged. Nevertheless, the effect of such methodologies on attitude accuracy would have to be tested reliably using longer data spans (e.g. several flight lines) with an accurate orientation reference.

CHAPTER 8

CONCLUSIONS AND RECOMMENDATIONS

The main objective of this research was to investigate INS/GPS integration for deriving precise attitude in support of airborne remote sensing and to assess its accuracy, which has not been successfully done in the past. The effect of measurement system errors on orientation accuracy has been analyzed using an attitude error model. The parameters of optimal integration for inertial sensors of different accuracy have been investigated in computer simulations. In-flight kinematic attitude performance obtained by integrating a strapdown inertial system and double differenced GPS measurements has been evaluated by comparison to orientation parameters derived from inverse photogrammetry. Based on this research, the following major conclusions can be drawn and the subsequent recommendations be made.

8.1 Conclusions

1. Aiding a strapdown Inertial Navigation System with DD GPS position and velocity substantially reduces the attitude errors.

2. The dominant systematic errors in INS-derived attitude are due to the initial misalignment, gyro drift and navigation (position, velocity) errors. These errors can be almost completely eliminated by frequent GPS updates, which are most effective in roll and pitch. The GPS update rate has to be chosen optimally, otherwise additional noise is introduced into the attitude due to GPS measurement noise. The optimal velocity and position update rate is about 50 and 40 seconds when integrating a strapdown INS from medium and medium-low accuracy class, respectively.
3. The dominant attitude errors of random type are caused mainly by gyro noise and synchronization errors. Even though the gyro noise level of the LTN-90-100, free of environmental disturbance, is as low as 3 arc seconds, it can be amplified up to 15 arc seconds in flight due to aircraft vibrations.
4. The short term (1 minute) orientation errors are 13, 34 and 30 arc seconds in aircraft roll, pitch and azimuth, respectively, using a medium accuracy INS. The larger error in pitch reflects non removable effects of a system misalignment due to a one second data discontinuity. Twenty percent of the derived orientation errors may also be due to the uncertainty in attitude reference used and 5 to 10 arcseconds due to INS-GPS synchronization errors.

5. Aerotriangulation at 1:10 000 photo scale with minimum ground control was demonstrated to be better than 10 cm RMS with respect to the surveyed control points. If long-term orientation accuracy of 15 -30 arc seconds can be confirmed in future tests, all but the most demanding engineering applications can be done with airborne georeferencing by INS/GPS. In that case, only a minimum of 4 control points on the ground would be needed for solving the relative orientation between the INS and the imaging sensor.

8.2 Recommendations

1. In order to confirm INS/GPS long-term attitude performance extended data sets need to be obtained in future flight tests.
2. Better results in short-term attitude determination can be expected when filtering techniques performing noise reduction would be developed and fine-tuned for vibrations of a specific aircraft. However, since such a method could generate systematic errors, testing on longer data sets would be preferable.
3. The synchronization between measurement systems should be improved to about 0.1 milliseconds to keep attitude errors resulting from synchronization errors below the noise level. Especially, the INS measurement delay needs to be carefully investigated when designing an INS/GPS system in support of airborne remote sensing.

4. To support the airborne sensor with INS/GPS derived attitude, a precise estimate of the orientation offset between the INS and the imaging sensors is needed. In frame-based imagery, this could be achieved by means of an on-the-fly calibration, as described in Section 7.2. Such a task is more complicated in the case of pushbroom imagery when the attitude and position parameters are required for each scan line. However, a specialized photogrammetric bundle adjustment making use of ground control points with conjugate points between overlapping images has been developed and successfully tested (Cosandier et al. 1994).

REFERENCES

- Ackermann F. and H. Schade** (1993) Application of GPS for Aerial Triangulation, *Photogrammetric Engineering and Remote Sensing PE & RS*, Vol. 59, No. 11, pp. 1625-1632.
- Blais, J.A.R.** (1979) Least-Squares Block Adjustment of Stereoscopic Models and Error Analysis, Ph. D. Thesis, Report Number 30001, Department of Geomatics Engineering, The University of Calgary.
- Britting, K.R.** (1971) Inertial Navigation System Analysis, Wiley-Interscience, New York.
- Cannon, M.E.** (1991) Airborne GPS/INS with an Application to Aerotriangulation, Report No. 20040, Department of Geomatics Engineering, The University of Calgary.
- Cannon, M.E., K.P. Schwarz and M. Wei** (1992) A Consistency Test of Airborne GPS Using Multiple Monitor Stations, *Bulletin Géodésique*, Vol. 66, No. 1, pp. 2-11.
- Cosandier, D.** (1994) GPSBUND & FORMSTRP - Software For Photogrammetric Block Adjustment, Reference Manual, Way Point Consulting Inc.

Cosandier, D., T.A. Ivanco, M.A. Chapman and M. Dylke (1994) The Integration of a Digital Elevation Model in *casi* Image Geocorrection, Presented at the First International Airborne Remote Sensing Conference and Exhibition, Strasbourg, France, September 11-15.

Czompo, J. (1990) Use of Spectral Methods in Strapdown ISS Data Processing, Proceedings of the International Symposium on Kinematic Systems for Geodesy, Navigation and Remote Sensing, Banff, September 10-14, Springer-Verlag, New York.

El-Mowafy, A. and K.P. Schwarz (1994), Epoch by Epoch Ambiguity Resolution for Real-Time Attitude Determination Using a GPS Multi-Antenna System in Kinematic Mode, Proc. KIS-94, Banff, Canada, August 30 - September 2, 1994.

Farrell, J.L. (1976) *Integrated Aircraft Navigation*, Academic Press, New York.

Gelb, A. ed. (1974) *Applied Optimal Estimation*, The M.I.T. Press, Cambridge, Massachusetts.

Hoffman, O. (1988) A Digital Three Line Stereo Scanner System, Archives of the Int. Society of Photogrammetry and Remote Sensing, Commission II, WGII/6, pp. 206-213.

Kenefick, J.K. (1972) Analytical Self-Calibration, *Photogrammetric Engineering*, Vo. 38, No. 11, November, pp. 1117-1126.

Lapucha, D. (1990) Precise GPS/INS Positioning for a Highway Inventory System, Report No. 20038, Department of Geomatics Engineering, The University of Calgary.

Liu, Z. (1992) Comparison of Statistical Methods for the Alignment of Strapdown Inertial Systems, Report No. 20047, Department of Geomatics Engineering, The University of Calgary.

Mader, G.L. and J.R. Lucas (1989) Verification of Airborne Positioning Using Global Positioning System Carrier Phase Measurements, *Journal of Geophysical Research*, Vol. 94, No. B8, pp. 10175-10181.

Remondi, B.W. (1985) Performing Centimeter Accuracy Relative Surveys in Seconds Using GPS Carrier Phase. Proc. of First International Symposium on Precise Positioning with the GPS, Rockville, Maryland, April 15-19.

Remondi, B.W. (1988) Kinematic and Pseudo-Kinematic GPS, Presented at the Int. ION GPS-88, Colorado Springs, Colorado, Sept. 19-23.

Savage, P.G. (1978) Strapdown Sensors, in AGARD Lecture Series No. 95, NATO, Neuilly sur Seine.

Schwarz, K.P., M.E. Cannon and R.V.C. Wong (1989) A Comparison of GPS Kinematic Models for the Determination of Position and Velocity Along a Trajectory, *Manuscripta Geodaetica*, Vol. 14, No. 5, pp. 345-353.

Schwarz, K.P. and M. Wei (1990) Testing a Decentralised Filter for GPS/INS Integration, Proceedings of the IEEE 1990 PLANS - Position, Location and Navigation Symposium, Las Vegas, Nevada, March 20-23.

Schwarz, K.P., M.A. Chapman, M.E. Cannon and P. Gong (1993) An Integrated INS/GPS Approach to the Georeferencing of Remotely Sensed Data, *Photogrammetric Engineering & Remote Sensing*, Vol. 59, No. 11, pp. 1667-1674.

Schwarz, K.P., M.V. Gelderen and M. Wei (1993) Integrated MAPS/GPS performance study, Scientific Services Program, Armament Research, Development and Engineering Center, Contract Report DAAL 03-91-C-0034.

Schwarz, K.P., M. Wei and M. Van Gelderen (1994) Aided Versus Embedded - A Comparison of two Approaches to GPS/INS Integration, Proceeding of the IEEE 1994 PLANS - Position, Location and Navigation Symposium.

Schwarz, K.P., M. A. Chapman, M.E. Cannon, P. Gong and D. Cosandier (1994) A Precise Positioning/Attitude System in Support of Airborne Remote Sensing, Proceeding of the GIS/ISPRS Conference, Ottawa, June 6-10.

Schwarz, K.P. and M. Wei (1994) ENSU 623 Lecture Notes, Department of Geomatics Engineering, The University of Calgary.

Schwarz, K.P. and M. Wei (1995) Modelling INS/GPS for Attitude and Gravity Applications, 3rd International Workshop of High Precision Navigation, Stuttgart, Germany, April 3-6.

Skaloud, J., D. Cosandier, K.P. Schwarz and M.A. Chapman (1994) GPS/INS Orientation Accuracy Derived From A Medium Scale Photogrammetry Test, International Symposium on Kinematic Systems in Geodesy, Geomatics and Navigation - KIS94, Banff, Canada, August 30 - September 2.

Wei, M. and K.P. Schwarz (1990) A Strapdown Inertial Algorithm Using an Earth-Fixed Cartesian Frame, *Navigation*, Vol 37, pp. 153-167.

Wei, M. and K.P. Schwarz (1990) Testing a Decentralized Filter for GPS/INS Integration, Proceedings of IEEE Position Location and Navigation Symposia, Las Vegas, Nevada, March 20-23, pp. 429-435.

Wolf, P.R. (1983) *Elements of Photogrammetry*, McGraw-Hill, Second Edition

Wong, R.V.C and K.P. Schwarz (1983) Dynamic Positioning with an Integrated GPS-INS
Formulae and Baseline Tests, Publication 30003, Department of Surveying
Engineering, The University of Calgary.

Wong, R.V.C. (1988) Development of a RLG Strapdown Inertial Survey System, Report
No. 20027, Department of Surveying Engineering, The University of Calgary.